

PREDICTING INJECTION SITE DRUG PRECIPITATION

by

Daniel C. Evans

A Dissertation Submitted to the Faculty of the

DEPARTMENT OF PHARMACEUTICAL SCIENCES

In Partial Fulfillment of the Requirements

For the Degree of

DOCTOR OF PHILOSOPHY

In the Graduate College

THE UNIVERSITY OF ARIZONA

2013

UMI Number: 3610739

All rights reserved

INFORMATION TO ALL USERS

The quality of this reproduction is dependent upon the quality of the copy submitted.

In the unlikely event that the author did not send a complete manuscript and there are missing pages, these will be noted. Also, if material had to be removed, a note will indicate the deletion.



UMI 3610739

Published by ProQuest LLC (2014). Copyright in the Dissertation held by the Author.

Microform Edition © ProQuest LLC.

All rights reserved. This work is protected against unauthorized copying under Title 17, United States Code



ProQuest LLC.
789 East Eisenhower Parkway
P.O. Box 1346
Ann Arbor, MI 48106 - 1346

THE UNIVERSITY OF ARIZONA

GRADUATE COLLEGE

As members of the Dissertation Committee, we certify that we have read the dissertation prepared by Daniel C. Evans, titled Predicting Injection Site Drug Precipitation and recommend that it be accepted as fulfilling the dissertation requirement for the Degree of Doctor of Philosophy.

Dr. Samuel H. Yalkowsky

Date: January 7th, 2014

Dr. Paul B. Myrdal

Date: January 7th, 2014

Dr. Michael Mayersohn

Date: January 7th, 2014

Dr. Joan Curry

Date: January 7th, 2014

Dr. Marcel Schaap

Date: January 7th, 2014

Final approval and acceptance of this dissertation is contingent upon the candidate's submission of the final copies of the dissertation to the Graduate College.

I hereby certify that I have read this dissertation prepared under my direction and recommend that it be accepted as fulfilling the dissertation requirement.

Dissertation Director: Dr. Samuel H. Yalkowsky

Date: January 7th, 2014

STATEMENT BY AUTHOR

This dissertation has been submitted in partial fulfillment of requirements for an advanced degree at The University of Arizona and is deposited in the University Library to be made available to borrowers under rules of the Library.

Brief quotations from this dissertation are allowable without special permission provided that accurate acknowledgment of source is made. Requests for permission for extended quotation from or reproduction of this manuscript in whole or in part may be granted by the head of the major department or the Dean of Graduate College when in his or her judgment the proposed use of the material is in the interests of scholarship. In all other instances, however, permission must be obtained from the author.

SIGNED: Daniel C. Evans

ACKNOWLEDGEMENTS

I would first and foremost like to thank my mentor Dr. Samuel H. Yalkowsky. You have worked so hard to give me a wonderful new life in science and to make graduate school the best years of my life. I could not repay in a hundred lifetimes what you have given me in this one.

I would also like to thank Dr. Paul Myrdal, Dr. Michael Mayersohn, Dr. Joan Curry, and Dr. Marcel Schaap for their guidance as doctoral committee members. I will always remember what a privilege it was to learn from you. To Dr. Mike Kudenov, thank you for all of your hard work that made the new in vitro device possible.

To my family and friends, thank you for your support and prayers that kept me afloat during graduate school. Finally, thank you God for giving me life and countless undeserved blessings.

DEDICATION

To my grandfather Toivo.

TABLE OF CONTENTS

INDEX OF TABLES	9
TABLE OF FIGURES.....	10
ABSTRACT.....	13
SPECIFIC AIMS	14
CHAPTER 1: INTRODUCTION.....	15
1.1. FACTORS AFFECTING PARENTERAL DRUG COMPATIBILITY	15
1.1.1. General Solubility	16
1.2. DRUG SOLUBILIZATION.....	16
1.2.1. pH Solubilization	17
1.2.2. Cosolvent Solubilization.....	18
1.2.2.1. Log-Linear Model.....	19
1.2.3. Other Solubilization Methods	20
1.3. DILUTION WITH BLOOD.....	22
1.3.1. Mixing.....	25
1.3.2. Precipitation Kinetics.....	26
1.4. IN VITRO PRECIPITATION TESTING.....	26
1.4.1. History.....	27
1.4.2. Current Dynamic Device	28
1.5. COMPUTATIONAL SOFTWARE.....	30

1.5.1. History and Current Software	30
CHAPTER 2: EXPERIMENTAL SECTION	32
2.1. NEW DYNAMIC IN VITRO DEVICE	32
2.1.1. New Flow Cell	32
2.1.2. Instrument Setup	33
2.1.3. Instrument Results	35
2.2. COMPUTATIONAL SOFTWARE.....	39
2.2.1. Computational Results	40
2.3. EXPERIMENTS	42
2.3.1. Initial Drug Study	42
2.3.2. Temperature Study.....	43
CHAPTER 3: RESULTS AND DISCUSSION	45
3.1. INITIAL DRUG STUDY RESULTS.....	45
3.1.1. Amiodarone Hydrochloride	45
3.1.1.1. Software Results	46
3.1.1.2. In Vitro Results	48
3.1.2. Phenytoin Sodium.....	52
3.1.2.1. Software Results	53
3.1.2.2. In Vitro Results	56
3.1.3. Verapamil HCl.....	59
3.1.3.1. Software Results	60

3.1.3.2. In Vitro Results	62
3.1.4. Proprietary Antibiotic	64
3.1.4.1. Software Results	65
3.1.4.2. In Vitro Results	69
3.1.5. Non-Precipitating Drugs	73
3.1.5.1. In Vitro Results	74
3.2. TEMPERATURE STUDY	77
SUMMARY	81
APPENDIX A – List of chemicals used for the in vitro study	82
REFERENCES.....	83

INDEX OF TABLES

Table 1. Comparison of current and new precipitation detection device	34
Table 2. Drugs Used for In Vitro device study	42
Table 3. Drugs Used for In Vitro temperature and serum albumin study.....	44
Table 4. Physical properties and chemical structure of amiodarone	45
Table 5. Physical properties and chemical structure of phenytoin	53
Table 6. Physical properties and chemical structure of verapamil	59
Table 7. Physical properties of the proprietary antibiotic and chemical structure of erythromycin	65
Table 8. Buffers used in proprietary antibiotic formulations.....	65
Table 9. Calculated AUC values from the intensity plots	69
Table 10. Negative control drugs used for testing the in vitro device	73
Table 11. Structures of epinephrine, clarithromycin, and furosemide.....	73
Table 12. Chemicals used for the in vitro study	82

TABLE OF FIGURES

Figure 1. pH-solubility plot for a weak acid drug.....	18
Figure 2. Plot of drug solubility vs. cosolvent fraction	19
Figure 3. Ethylbenzene solubility vs. surfactant concentration	21
Figure 4. Griseofulvin solubility vs. cyclodextrin concentration	21
Figure 5. pH vs. formulation fraction for phenytoin formulations	23
Figure 6. Drug concentration vs. formulation fraction for phenytoin formulations	24
Figure 7. Drug concentration and solubility plot for phenytoin formulations	25
Figure 8. 1:1 serial dilution assay for drug precipitation	28
Figure 9. In vitro device to detect drug precipitation (25).....	29
Figure 10. New in vitro device flow cell design.....	33
Figure 11. New in vitro device setup.....	34
Figure 12. Image of the flow cell near the IV needle	36
Figure 13. Scaled intensity image of flow cell	36
Figure 14. Image taken during an injection with no drug precipitation.....	37
Figure 15. Image taken during injection with drug precipitation	38
Figure 16. Scaled intensity image after injection of phenytoin sodium	39
Figure 17. Drug solubility and blood dilution program GUI.....	40
Figure 18. Equations used in the solubility and blood dilution software.....	41
Figure 19. Buffer capacity of ISPB.....	43
Figure 20. pH-solubility curve for amiodarone	47
Figure 21. pH-dilution curve for amiodarone HCl	47

Figure 22. Drug concentration and solubility plot for amiodarone HCl.....	48
Figure 23. In vitro results for amiodarone HCl.....	49
Figure 24. Image of the needle tip during the 1ml/min placebo amiodarone injection	50
Figure 25. Image of the needle tip during the 1ml/min active amiodarone injection.....	50
Figure 26. Image of the 1ml/min amiodarone injection downstream.....	51
Figure 27. Image of the 5ml/min amiodarone injection downstream.....	52
Figure 28. pH-solubility plot for phenytoin.....	54
Figure 29. pH-dilution curve for phenytoin sodium.....	55
Figure 30. Drug concentration and solubility plot for phenytoin sodium.....	55
Figure 31. In vitro results for phenytoin sodium 50 mg/ml.....	57
Figure 32. Image of needle tip during a 0.5 ml/min injection of phenytoin sodium.....	57
Figure 33. Image of the needle tip during the 1ml/min phenytoin sodium injection.....	58
Figure 34. Downstream image of the 1ml/min phenytoin sodium injection.....	58
Figure 35. pH solubility plot for verapamil.....	60
Figure 36. pH-dilution curve for verapamil HCl.....	61
Figure 37. Drug concentration and solubility plot for verapamil HCl.....	61
Figure 38. In vitro results for verapamil HCl.....	62
Figure 39. Image of needle tip for 1ml/min verapamil HCl injection.....	63
Figure 40. Image of 1ml/min verapamil HCl injection downstream.....	63
Figure 41. Image of 5ml/min verapamil HCl injection downstream.....	64
Figure 42. pH-solubility plot for the proprietary antibiotic.....	66
Figure 43. Buffer capacity of proprietary antibiotic formulations.....	67

Figure 44. pH-dilution curve for proprietary antibiotic formulations.....	68
Figure 45. Drug concentration & solubility plot for the proprietary antibiotic	68
Figure 46 In vitro results for the proprietary antibiotic formulations.....	69
Figure 47. In vitro results for the proprietary antibiotic formulations.....	70
Figure 48. Image of proprietary antibiotic (form 1) at the needle tip	71
Figure 49. Image of the proprietary antibiotic (form 2) at the needle tip	71
Figure 50. Image of the proprietary antibiotic (form 1) downstream	72
Figure 51. Image of the proprietary antibiotic (form 2) downstream	72
Figure 52. In vitro results for clarithromycin lactobionate	74
Figure 53. In vitro results for epinephrine	75
Figure 54. In vitro results for furosemide	76
Figure 55. In vitro results for amiodarone HCl (ISPB at 25 ⁰ C and 37 ⁰ C).....	77
Figure 56. In vitro results for phenytoin sodium (ISPB at 25 ⁰ C and 37 ⁰ C).....	78
Figure 57. In vitro results for verapamil HCl (ISPB at 25 ⁰ C and 37 ⁰ C).....	78
Figure 58. Image of the 1ml/min amiodarone HCl injection (ISPB at 37 ⁰ C).....	79
Figure 59. Image of 1ml/min phenytoin sodium injection (ISPB at 37 ⁰ C)	79
Figure 60. Image of the 1ml/min verapamil HCl injection (ISPB at 37 ⁰ C).....	80

ABSTRACT

Administering drug therapy through the intravenous route ensures rapid, and complete, bioavailability, which can be critical in an emergency situation. However, bypassing all of its protective barriers leaves the body vulnerable to harm if the parenteral formulation becomes unstable when mixed with the blood. An example of this formulation instability is the precipitation of poorly water-soluble drugs after mixing with the blood's aqueous environment. This happens when parenteral formulations rely too heavily upon the solution pH, and excipients, to increase the drug solubility. This precipitation in the blood can damage venous cell membranes producing symptoms ranging from mild skin irritation to death.

To screen potential drug formulations for problems such as injection site drug precipitation, pharmaceutical companies have traditionally used costly and time consuming animal studies. To reduce the amount of pre-clinical animal studies necessary to find an optimal IV formulation, an in vitro device to detect injection site drug precipitation is introduced. In addition to the device, software that simulates the dilution of a parenteral drug formulation with blood upon administration has been developed and is introduced. Both the device and software were tested on commercially available formulations plus one formulation currently in clinical trials. The results and capabilities of the new device were compared to those obtained using an earlier in vitro device. Finally, a robust model for early screening of injection site precipitation is developed using both the in vitro device and software.

SPECIFIC AIMS

The overall goal of this study is to develop a model that will accurately predict the precipitation of parenteral drugs upon mixing with blood. This will be accomplished by completing the following.

- The first aim of this study is to develop an in vitro device that simulates IV administration of a drug into the bloodstream, and is capable of detecting the occurrence of precipitation of drug at the needle tip. The device will be tested with commercially available drug formulations that are known to cause, or not cause, phlebitis. Additionally we will investigate if raising the temperature of our blood surrogate from 25⁰C to 37⁰C will significantly affect the in vitro results.
- The second aim of this study is to develop a software package that will enable the user to evaluate the performance of a drug formulation upon dilution with either blood or a pre-injection diluent. This software will predict the solubilization of drugs in commonly used pharmaceutical excipients and simulate the simultaneous drop in concentration and solubility upon dilution of the formulation.

This model will aid in the development of new formulations with reduced potentials for inducing phlebitis.

CHAPTER 1: INTRODUCTION

Intravenous (IV) drug delivery provides faster, and more complete bioavailability than any other route of administration (1). However, because IV administration bypasses all of the body's external barriers, a physical incompatibility between the drug formulation and the blood may cause damage to venous endothelial, and red blood cells. This damage can result in a condition called post-infusion, or post-injection phlebitis (PIP), which has symptoms ranging from mild discomfort to death (2). In the hospital setting, PIP is the most common cause of IV therapy morbidity, affecting 25-70% of all patients (3). To prevent the occurrence of phlebitis, pharmaceutical companies have historically used costly and time consuming animal testing to screen potential formulations. Developing in vitro and computational models to augment animal testing for infusion related problems will help the pharmaceutical industry meet the future increased demand for new parenteral drug formulations. Before introducing the models it is essential to better understand the factors that can affect parenteral drug stability.

1.1. Factors Affecting Parenteral Drug Compatibility

One of the main sources of physical incompatibility between parenteral formulations and blood is the solubility change that occurs immediately upon drug administration (4). Many of the approved parenteral formulations contain inactive ingredients, or excipients, to increase the solubility of the active drug. Upon mixing with blood, both the drug and the formulation excipients undergo dilution. This mixing simultaneously introduces blood components and reduces the concentration, and often the solubility, of the drug. If the rate at which the drug solubility decreases is greater than that of the concentration

decrease a transient supersaturated solution will occur near the site of injection. This supersaturated solution can produce solid drug particles in the blood which can delay bioavailability, damage venous cell membranes, and potentially cause thrombophlebitis.

1.1.1. General Solubility

The blood plasma is made up of approximately 90% water (5), and therefore the aqueous solubility of a drug is critical for its successful intravenous delivery. Drug absorption and activity, however, favor non-polar molecules with limited aqueous solubility. The solubility, S_w , of any non-electrolyte drug solute in an aqueous solution can be estimated by the General Solubility Equation (GSE) from Yalkowsky (6):

$$\log S_w = -0.01(MP-25) - \log K_{ow} + 0.5 \quad (1)$$

Where MP and K_{ow} are the drug's melting point in degrees centigrade and octanol-water partition coefficient respectively. The first term in the GSE reflects the energy required in the solid-liquid phase transition of the drug solute while the second term represents the difference in the polarity of the solute and the polar aqueous solution. Thus, assuming similar melting points, polar solutes are more soluble in aqueous media than non-polar solutes with the latter being more strongly squeezed out by self-associating water molecules.

1.2. Drug Solubilization

Because the majority of drug molecules are nonpolar, many methods have been developed to increase their aqueous solubility. Two of the most common methods, which are discussed in more depth below, are: changing the pH of the formulation and the

addition of a cosolvent (6). These two methods are important because they can increase the solubility of a drug exponentially, as opposed to the linear increases in solubility obtained with the use of other solubilization techniques. As seen later, this dramatic increase in solubility is lost upon dilution with blood, potentially creating a transient supersaturated solution that could result in drug precipitation.

1.2.1. pH Solubilization

If a parenteral drug has one or more ionizable functional groups its solubility can be increased by changing the pH of the formulation solution relative to the drug's pKa. For a drug with one acidic functional group, this increase in solubility is given by (7):

$$S_w^{\text{tot}} = S_w(1 + 10^{\text{pH} - \text{pKa}}) \quad (2)$$

Where S_w^{tot} is the total drug solubility at the solution pH, and S_w is the intrinsic aqueous solubility of the drug. Figure 1 shows a graph of equation 1 for a weak acid drug ($S_w = 10^{-3}\text{M}$, $\text{pKa} = 4.33$). The plateau in Figure 1 represents the solubility product (K_{sp}) of the salt that forms between the ionized drug and the buffer ion and can be described with the following equation (7):

$$S_w^{\text{tot}} = (1 + 10^{\text{pKa} - \text{pH}}) \sqrt{K_{\text{sp}}} \quad (3)$$

Similar equations for S_w^{tot} can be derived for drugs that are zwitterions or weak bases.

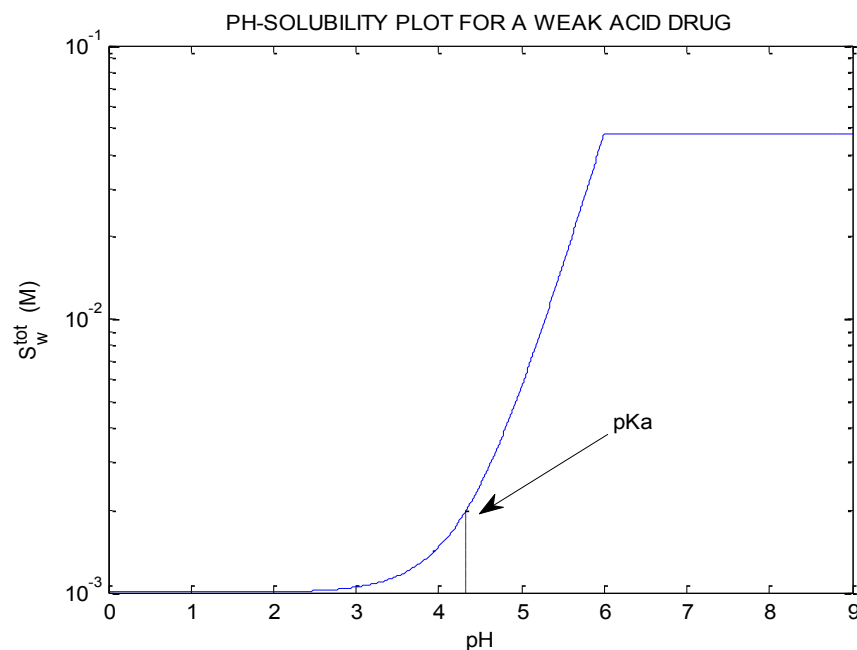


Figure 1. pH-solubility plot for a weak acid drug

1.2.2. Cosolvent Solubilization

If a nonpolar drug has no acidic or basic functional groups, its solubility can be increased exponentially by adding a water-miscible organic solvent to lower the polarity of the solution (8). The chemical structure of these cosolvents typically includes a small polar headgroup capable of forming hydrogen bonds, and a small hydrocarbon tail. This structure allows the cosolvent to interact and disrupt the aqueous hydrogen bonding network, thereby reducing water's ability to squeeze out non-polar solutes. To describe the solubility of a nonpolar drug in a mixture of water and commonly used pharmaceutical cosolvents, the simple and well developed log-linear model of Yalkowsky (9) is used.

1.2.2.1. Log-Linear Model

The log-linear model, from Yalkowsky (9), gives the total solubility of a nonelectrolyte drug in a cosolvent-water mixture, S_{mix} , as a function of the solubilization power, σ , and the fraction of cosolvent, f_c :

$$S_{\text{mix}} = S_w + 10^{\sigma f_c} \quad (4)$$

Where the solubilization power, σ , for a nonelectrolyte drug is related to its partition coefficient by cosolvent-dependent constants A and T by:

$$\sigma = A \log K_{ow} + T \quad (5)$$

Figure 2 shows a solubility plot for a nonpolar drug ($\log K_{ow} = 2$ $\log S_w = -3$) in an ethanol-water mixture using empirically derived A and T values (6). For semi-polar solutes and high cosolvent fractions the solubility may deviate from the log-linear relationship.

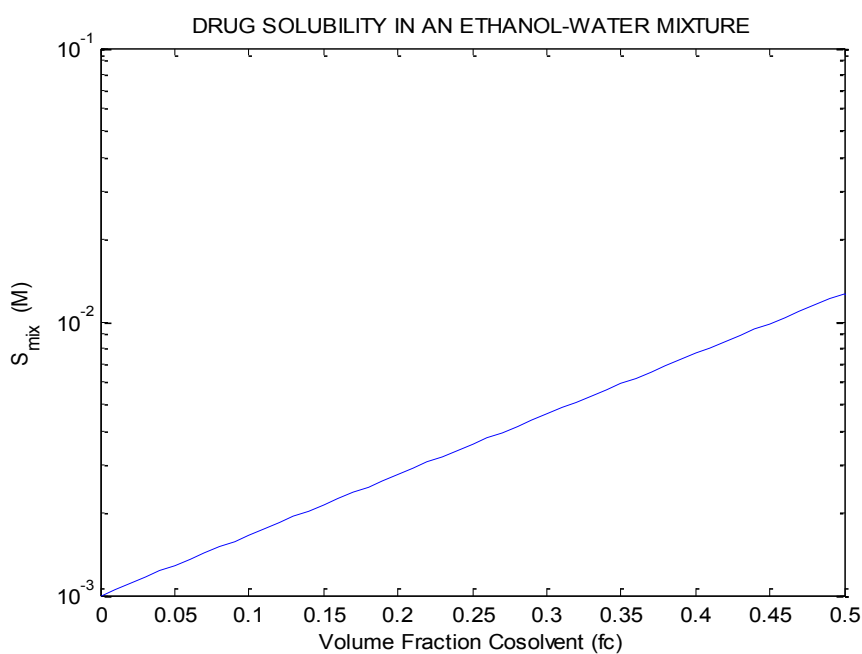


Figure 2. Plot of drug solubility vs. cosolvent fraction

1.2.3. Other Solubilization Methods

While not as common and versatile as the control of pH, or the use of cosolvents, the solubilization of nonpolar drugs by surfactants and complexation agents remains an important part of drug formulation. The total solubility, S_{mw}^{tot} , of a nonpolar drug as a function of the concentration of micellar surfactant (C_{surf}) is given by (6):

$$S_{mw}^{tot} = S_w + \kappa(C_{surf} - CMC) \quad (6)$$

Where κ is the solubilization capacity and the CMC (critical micelle concentration) is the concentration at which the surfactant begins to form drug solubilizing micelles.

The total solubility, S_{cd}^{tot} , of a nonpolar drug in an aqueous solution containing a ligand, such as a cyclodextrin, that forms a 1:1 complex given by:

$$S_{cd}^{tot} = S_w + \left(\frac{K_{1:1} S_w [L]_T}{1 + K_{1:1} S_w} \right) \quad (7)$$

With S_w representing the aqueous solubility of the free solute, $[L]_T$ is the total ligand concentration, and:

$$K_{1:1} = \frac{[DL]}{[D]_F [L]_F} \quad (8)$$

Where $[D]_F$ and $[L]_F$ are the concentrations of free drug and free ligand, and $[DL]$ is the concentration of the drug-ligand complex. Figure 3 (10) is a plot showing the solubility increase for ethylbenzene as a function of ligand concentration for two micellar surfactants. Figure 4 (11) is a plot showing the solubility increase for the antifungal drug griseofulvin as a function of ligand concentration for two cyclodextrins.

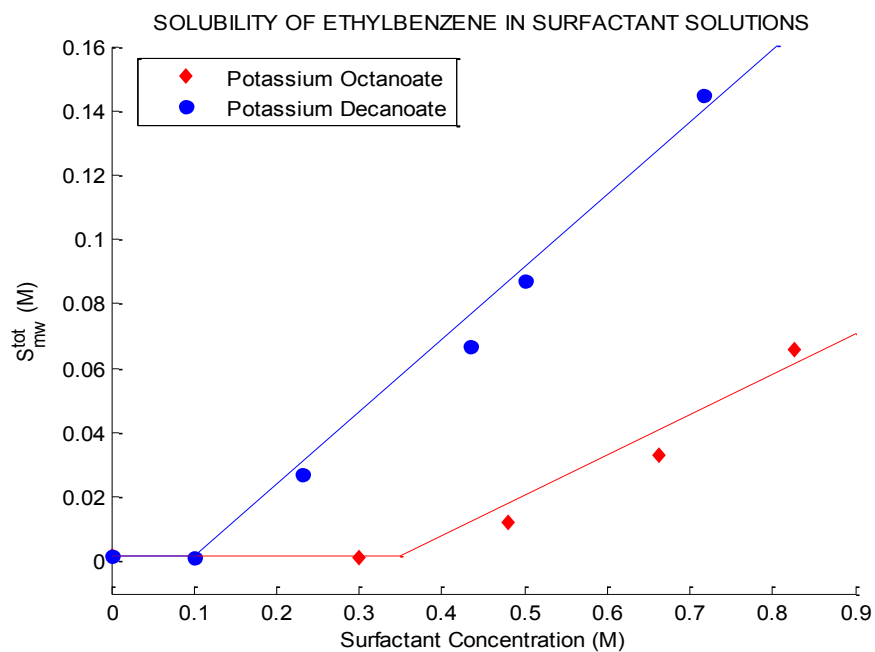


Figure 3. Ethylbenzene solubility vs. surfactant concentration

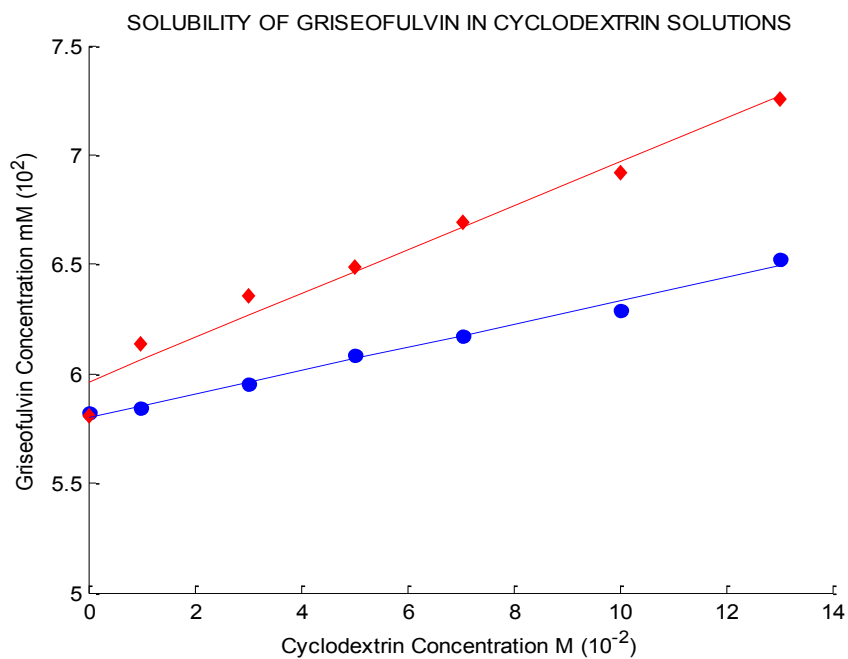


Figure 4. Griseofulvin solubility vs. cyclodextrin concentration

1.3. Dilution With Blood

Human blood is a complex fluid where red blood cells are suspended in an aqueous solution containing proteins, mineral ions, glucose, and other components (12). These components regulate the tonicity of the blood, and keep the pH in the narrow range of 7.35-7.45. If a parenteral drug is formulated outside the normal blood pH range, that formulation, upon mixing, will undergo both dilution and titration simultaneously (13). To plot this titration of drug formulation sodium phosphate is used to model the buffering capacity of blood and the general titration functions of de Levie (14).

$$f_f = \frac{V_{\text{FORM}}}{V_{\text{FORM}} + V_{\text{BLOOD}}} = \frac{-\sum F_{\text{BLOOD}} C_{\text{BLOOD}} - [\text{H}^+] + [\text{OH}^-]}{\sum F_{\text{FORM}} C_{\text{FORM}} - \sum F_{\text{BLOOD}} C_{\text{BLOOD}}} \quad (9)$$

Where the volume fraction of formulation (f_f) is a function of the hydrogen ion concentration, the molar concentrations of the phosphate blood surrogate (C_{BLOOD}), and formulation electrolytes (C_{FORM}), and the buffer function F :

$$-F_{\text{ACID}} = F_{\text{BASE}} = \frac{\sum_{j=0}^p (p-q-j) [\text{H}^+]^{p-j} \prod_{i=0}^j K_i}{\sum_{j=0}^p [\text{H}^+]^{p-j} \prod_{i=0}^j K_i} \quad (10)$$

With p , and q , defined as the maximum and actual number of protons for the weak acid or base respectively. Figure 5 shows a plot of pH vs. the formulation fraction for phenytoin ($\text{pK}_a=8.33$) formulated at pH 11 with, and without, a sodium phosphate buffer. The 1 and 0 on the horizontal axis represent the formulation before dilution and at infinite dilution, with the sodium phosphate blood surrogate respectively. This figure shows that the pH of an unbuffered formulation is rapidly titrated to 7.4 in the body, while the formulation with the higher buffer concentration maintains a higher pH until further

dilution. Because this change in pH can lead to an exponential decrease in solubility of a weak electrolyte drug, a small amount of buffer can be a very useful excipient. Figure 6 is a plot of solubility vs. the fraction of formulation for formulations of phenytoin calculated from the pH of figure 5.

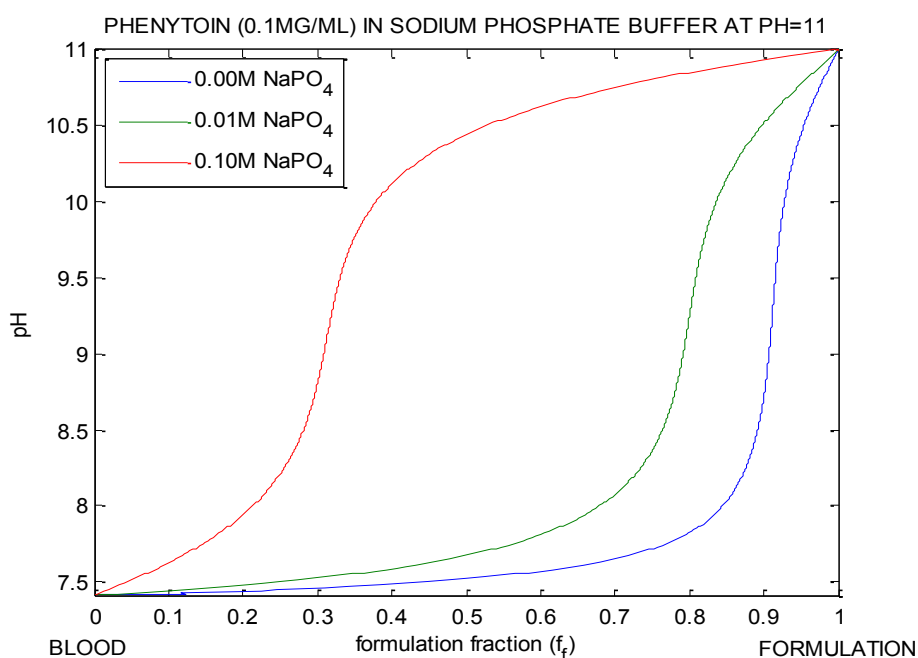


Figure 5. pH vs. formulation fraction for phenytoin formulations

In addition to titrating, the blood also dilutes the concentration of drug and all excipients used in the formulation. The final concentration of the formulation contents during the dilution, C_f , is the product of the formulation fraction and the initial formulation concentration, C_i .

$$C_f = C_i \cdot f_f \quad (11)$$

When a cosolvent is used in a parenteral formulation, the linear decrease in cosolvent concentration, or fraction ($fc_f = fc_i \cdot f_f$), can exponentially reduce the solubility of a nonpolar drug.

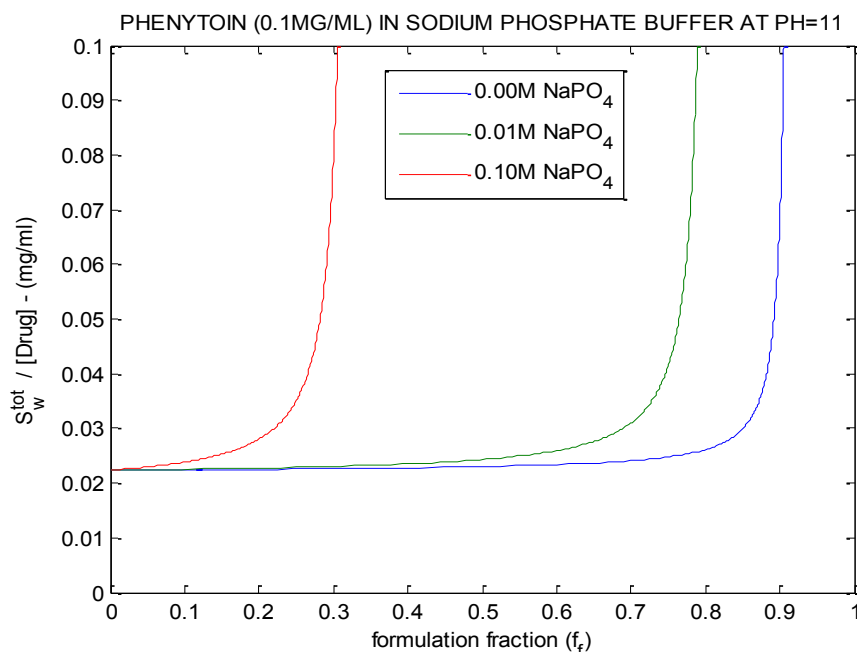


Figure 6. Drug concentration vs. formulation fraction for phenytoin formulations

Superimposing the plot shown in figure 6, and a plot of drug concentration vs. formulation fraction (equation 11), reveals areas of supersaturation for a drug during the dilution process. An example of this superimposed solubility and concentration plot for buffered and unbuffered phenytoin (0.1mg/ml) is shown in figure 7 where the areas of supersaturation are shaded. This plot demonstrates that for phenytoin, as the buffer concentration is increased, the area of supersaturation decreases. This supersaturated solution that occurs upon mixing a formulation with blood can result in solid drug particles coming out of solution. To determine whether or not this will occur, it is important to review the kinetics of precipitation along with the assumptions that are implicit in the calculations.

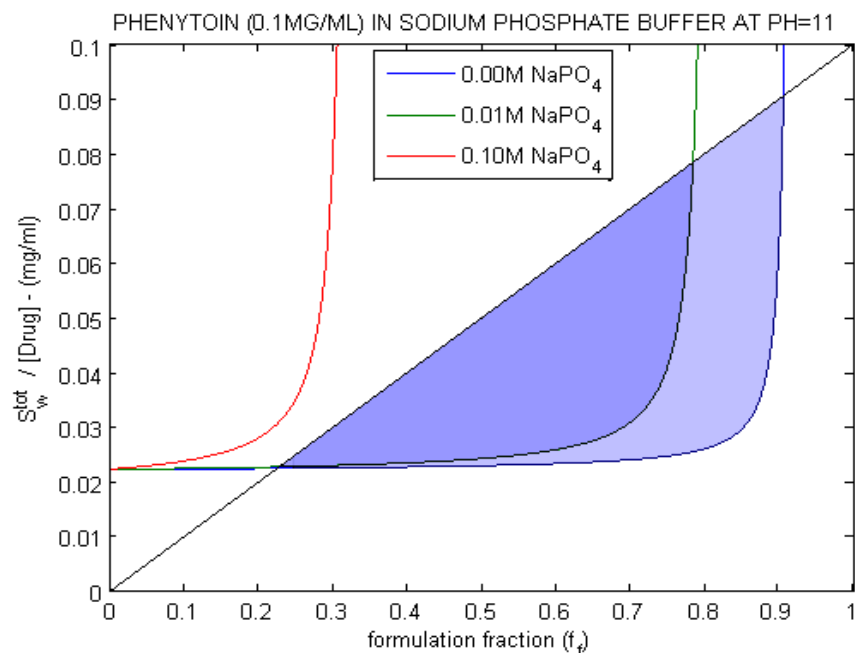


Figure 7. Drug concentration and solubility plot for phenytoin formulations

1.3.1. Mixing

The plot shown in figure 7 predicts the solubility and concentration of phenytoin that would be obtained from a static dilution with sodium phosphate buffer. Relating this data to an injection of phenytoin into the bloodstream requires knowledge of how the formulation mixes with blood at the site of injection. If complete mixing occurred at the site of injection the formulation fraction could be approximated as the ratio of injection rate to the sum of the injection rate and the blood flow rate. It is probably safer to assume that some of the formulation is completely mixed with blood at the site of injection while the rest of the formulation undergoes complete mixing downstream.

1.3.2. Precipitation Kinetics

The formation of a transient supersaturated solution upon parenteral drug administration does not always lead to precipitation. The formation of solid drug particles is preceded by an induction time (t_{ind}) which varies for different solutes. The equation that relates the induction time to the degree of supersaturation is given by (15):

$$t_{ind} = \frac{K}{\sigma^n} \quad (12)$$

Where K is a constant relating the induction time to the kinetic “order” of supersaturation (n), and the supersaturation ratio (σ) defined as:

$$\sigma = \frac{[D]}{S_w^{tot}} \quad (13)$$

This ratio of the drug concentration, [D], to the total solubility of the drug, S_w^{tot} , is a function of the vertical distance separating the concentration and solubility lines in figure 7. While the induction time is inversely related to the degree of supersaturation, it is also solute dependent and cannot be predicted. Therefore, it is reasonable to assume that an increase in the area of supersaturation for different formulations containing the same drug would increase the probability of drug precipitation.

1.4. In Vitro Precipitation Testing

Pre-clinical pharmaceutical studies cost an estimated 335 million (in year 2000 dollars) per approved new molecule (16) (17). Because animal testing is an expensive and time consuming process, the development of in vitro models to predict the performance of drug formulations has become an important part of the pharmaceutical industry. In vitro

drug dissolution / precipitation testing for oral drug formulations started around the 1950's (18). Since that time oral drug dissolution / precipitation testing has become standardized and an important requirement by regulatory agencies in the drug approval process (18). Despite this fact, the pharmaceutical literature contains very few in vitro methods to predict parenteral drug precipitation upon mixing with blood. The remainder of this chapter contains a brief literature review on the subject on in vitro testing for drug precipitation. Since a comprehensive literature review on the subject of in vitro testing for drug precipitation has already been published (19), this review will primarily focus on the studies that served as the building blocks for the new device and software.

1.4.1. History

Essentially, all models are wrong, but some are useful. –George Box (20)

The first recorded attempt to quantitate drug precipitation upon mixing with blood was a single-step dilution of phenytoin with human plasma published by Schroeder and DeLuca (21). Later other static methods such as the 1:1 serial dilution (figure 8) and the dropwise static assays (22), were developed to simulate dilution of parenteral formulations both in blood, and in pre-infusion diluents.

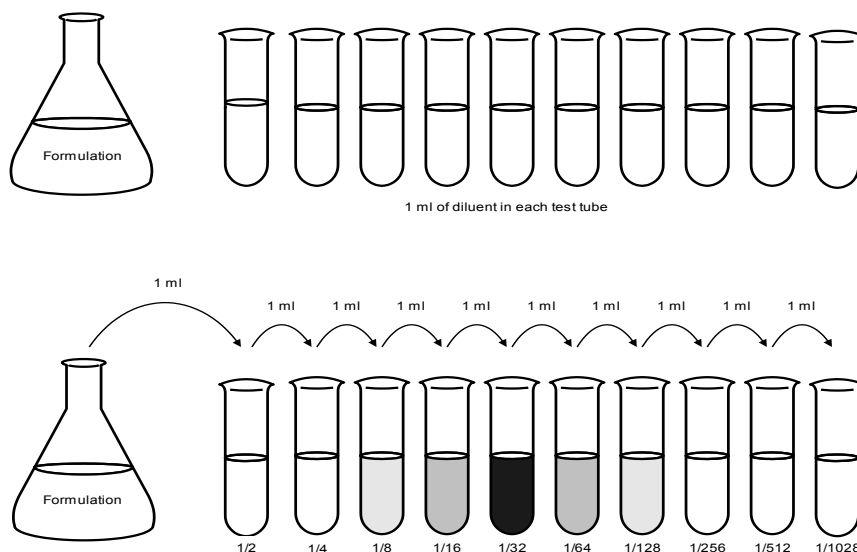


Figure 8. 1:1 serial dilution assay for drug precipitation

While these static experiments are simple to perform and provide rapid results, they do not take into account any of the fluid dynamics of administering a formulation directly into the bloodstream. Thus, static testing is more useful in the qualitative comparison of drug formulations and in the assessment of formulation compatibility with pre-infusion diluents.

1.4.2. Current Dynamic Device

Yalkowsky and Valvani (23) developed the first dynamic in vitro device to study the precipitation behavior of parenteral formulations of alprazolam and diazepam upon injection. Later Yalkowsky (24) and Johnson (25), improved, and validated the most well-known dynamic device shown in figure 9. This device simulates blood flow using a peristaltic pump that directs isotonic phosphate buffer (ISPB) at pH 7.4 through Tygon[®] tubing into a spectrophotometer flow cell. Parenteral formulations are then administered

upstream of the flow cell using an IV Y-site and a syringe pump. If a drug precipitates upon mixing with the blood surrogate, the solution passing through the flow cell will block the light and be recorded by the spectrophotometer as absorbance. To capture only precipitation, and not absorbance by the chemicals in solution, the spectrophotometer diode array is set to detect in visible region of the electromagnetic spectrum ($>500\text{nm}$).

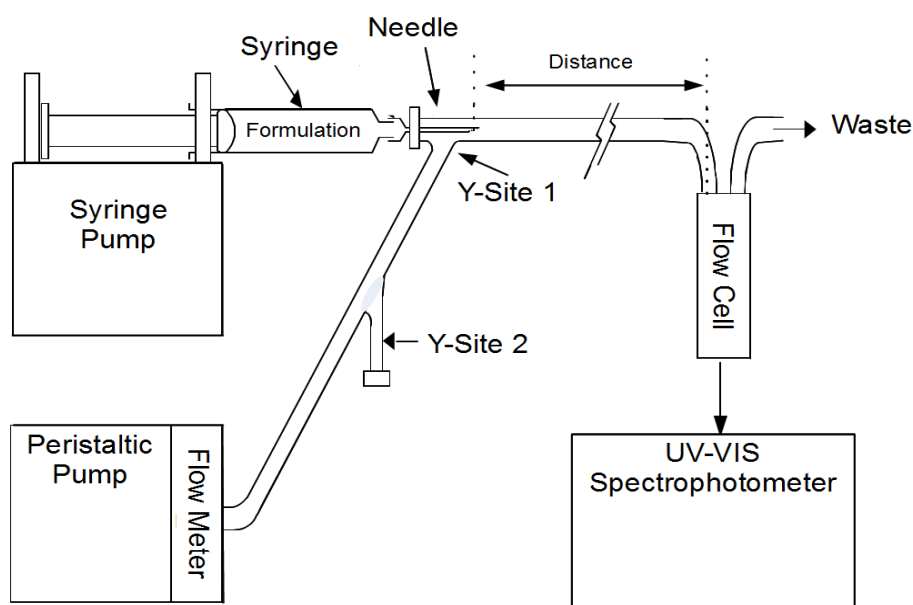


Figure 9. In vitro device to detect drug precipitation (25)

Using a spectrophotometer and flow cell to simulate injecting a formulation into the bloodstream has some limitations. To maximize the area of detection, the diameter and shape of most spectrophotometer flow cells are not optimal for simulating the veins of the arm. Using a U-shaped flow cell can become problematic if the precipitation cannot escape the effects of gravity or the flow eddies that have been observed in studies using

the previous device. Positioning the detector near the needle tip, where phlebitis is observed, is also difficult with a typical spectrophotometer and U-shaped flow cells. Other problems encountered with the current device include air bubbles and Schlieren patterns that absorb light and give false absorbance readings. These Schlieren patterns, caused by the mixing of fluids with different refractive indexes, have made it necessary to move the flow cell downstream in the validated in vitro device (25). Finally the detection of precipitation using a light absorbance detector is limited in the information that it can provide. Distinguishing between the formation of solid particles and a haze of precipitate can only be done through visual observation which is difficult through polymer tubing. The new in vitro device to simulate drug administration into the blood was designed to be able to detect drug precipitation at the needle tip.

1.5. Computational Software

1.5.1. History and Current Software

Surakitbanharn (13) developed the first Quattro Pro spreadsheet-based software for the prediction of parenteral drug precipitation. These calculations used isotonic phosphate buffer (ISPB) as the blood model and citrate and phosphate buffered formulations of phenytoin, dexverapamil (26), and levemopamil (27). Later Narazaki (28) (29) developed an Excel-based spreadsheet that took into account cosolvent and pH controlled solubility and allowed the user to choose an acid or base as a buffer.

The use of spreadsheets to predict the effect of blood dilution on drug solubility becomes more difficult as the complexity of the formulation increases. Using different combinations of solubilization techniques often requires the user to create new

spreadsheets. Also, the storage of excipient information such as physical constants along with the inherent number of iterations in titration and pH calculations requires the use of multiple worksheets. The new precipitation prediction software will feature a graphical user interface and eliminate the use of spreadsheets for the calculations.

CHAPTER 2: EXPERIMENTAL SECTION

2.1. New Dynamic In Vitro Device

The new dynamic in vitro device for detecting drug precipitation was created by replacing the flow cell, the light source, and detector on the current device. The flow cell was designed to allow detection of small amounts of drug precipitation at the needle tip as well as downstream. The components and positioning of the light source and detector were chosen to eliminate sources of instrumental error caused by Schlieren patterns and air bubbles. The other components of the instrument such as the peristaltic and syringe pump remain the same as in the statistically validated model (25).

2.1.1. New Flow Cell

Figure 10 shows a depiction of the newly designed flow cell. This flow cell was constructed by placing a round 4mm inner diameter fused quartz tube inside a larger rectangular quartz tube. The size of the inner quartz tube was selected to represent the inner diameter of the forearm Basilic vein (30). An IV Y-site was fastened to one end of the inner round quartz tube using polymer glue and the other end was attached to 4mm Tygon[®] tubing. Before sealing the ends of the rectangular tube, polyethylene glycol 200, which has an almost identical index of refraction (1.4585) (31) as quartz glass (1.458404) (32), was used to fill in the space between the two tubes. This design minimizes the effect of reflected and refracted light off the curved surface of the inner quartz tube and increases the sensitivity of the instrument.

FLOW CELL DESIGN

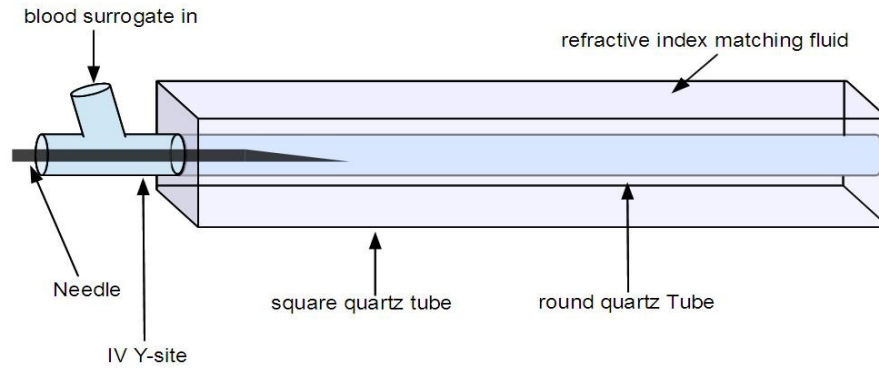


Figure 10. New in vitro device flow cell design

2.1.2. Instrument Setup

Figure 11 shows complete instrument setup. Two flexible fiber optic light guides illuminated by Vlux-1000 light source were positioned above the flow cell at approximately a 45 degree angle normal to the flow cell. The Imaging Source DMK 41BUO2 monochrome charge-coupled device (CCD) camera was positioned to the side of the flow cell approximately 90° from the incident light. A Nikon AF Nikkor 28-80mm lens SLR lens was attached to the camera with a 21mm lens tube. Both the light source and the camera were attached to a linear motion system constructed from T-slot aluminum extrusion so that images may be taken at the needle tip and downstream.

Table 1 gives a summary comparison of the major components of the current and new in vitro device for detecting parenteral drug precipitation upon administration.

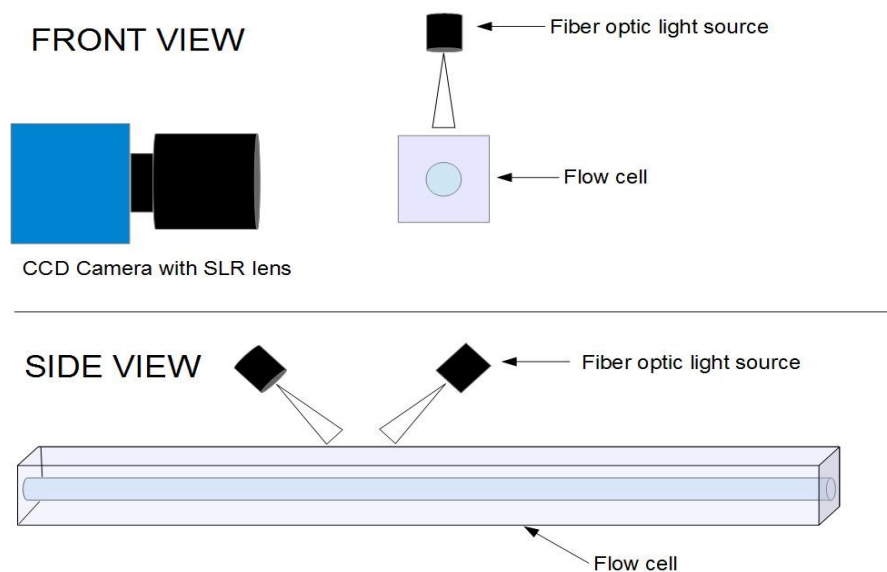


Figure 11. New in vitro device setup

Table 1. Comparison of current and new precipitation detection device

Element	Current Device	New Device
Light source	Xenon lamp	Vlux 1000 White Fiber Optic light source
Detector	Photodiode array	The Imaging Source® USB CCD Camera
Flow cell	Standard u-shaped cuvette cell	Newly designed flow cell (figure 10)
Detection Software	Cary UV-Win©	IC Capture Software© (The Imaging Source®)
Analysis Software	Cary UV-Win©	Image Processing Toolbox (Matlab®)

The in vitro experimental design was similar to that of the validation study done by Johnson and Yalkowsky (25). The ISPB (pH=7.4) blood surrogate was directed through 4mm Tygon® tubing into the flow cell at 5ml/min using the Cole Parmer Masterflex® peristaltic pump. A Harvard Apparatus® syringe pump was used to administer drug formulations at specified rates into the flowing ISPB. A popper 22 gauge 4" deflected point needle, attached to the syringe using small diameter tubing, was inserted into the IV Y-site attached to the flow cell. When a drug precipitated during administration the amount of scattered light reaching the camera increased proportionally to the amount of precipitation. The tubing exiting the flow cell passed through a variable area flow meter and into a waste container. Flow rates taken from the flow meter were confirmed with a 10ml graduated cylinder and a stopwatch. The CCD camera, using the IC Capture software package, was set to take images at one second intervals for a total of 1 minute during the infusion.

2.1.3. Instrument Results

Figure 12 is an image of the flow cell near the needle tip before any image processing is done. All of the images taken during the in vitro tests were loaded into the Matlab® software using the Image Processing Toolbox. The toolbox allows the scaling of these images according to the light intensity and displaying them in color. Figure 13 is the same image as shown in figure 12 with the light intensity values scaled from 0 to 255. In these images the darker blue colors represent low light intensity and the yellow and red colors represent higher light intensity values.

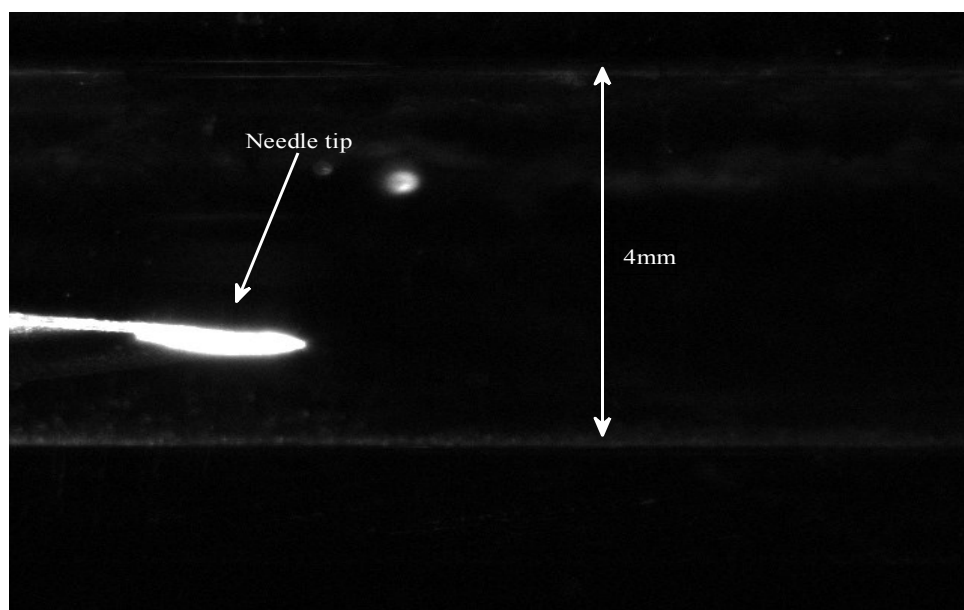


Figure 12. Image of the flow cell near the IV needle

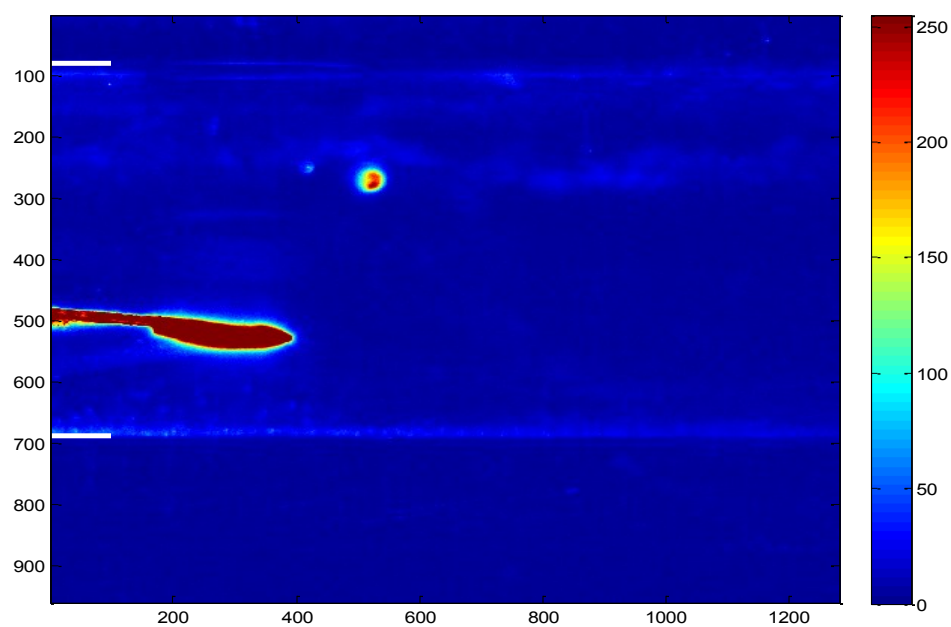


Figure 13. Scaled intensity image of flow cell

The images taken during the injection of formulations without drug (placebo) were subtracted from the images taken during the injection of the formulations containing active drug.

$$\text{Image}_{\text{Final}} = \text{Image}_{\text{Active}} - \text{Image}_{\text{Placebo}} \quad (14)$$

After background subtraction, the images were displayed in the scaled intensity format.

If there were any drug precipitation during the simulated injection, it would show up as colors ranging from lighter blue (low precipitation) to red (high precipitation). Figure 14 is a scaled intensity image where the drug did not precipitate after being injected. Figure 15 is a scaled intensity image where the drug did precipitate after being injected.

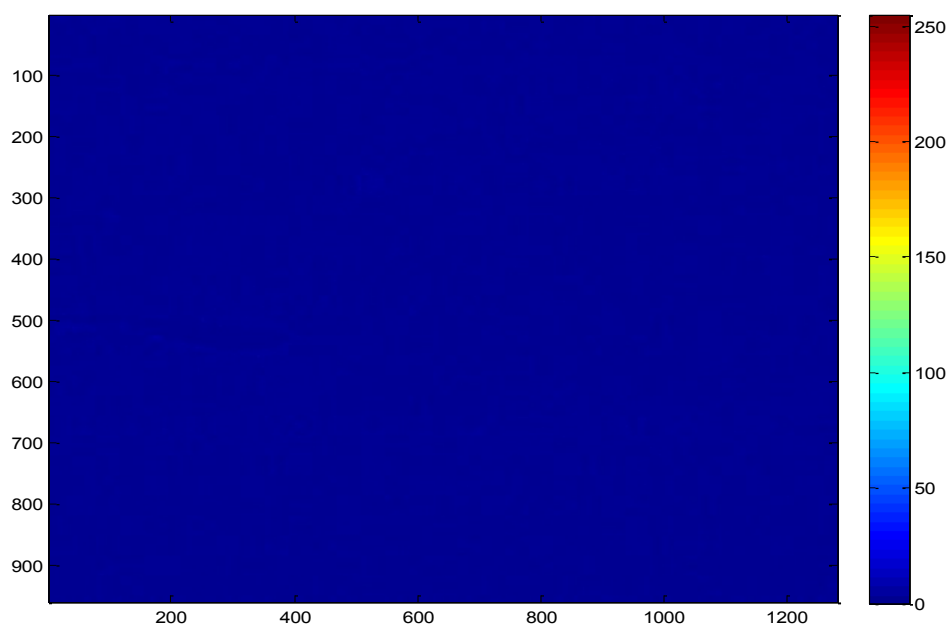


Figure 14. Image taken during an injection with no drug precipitation

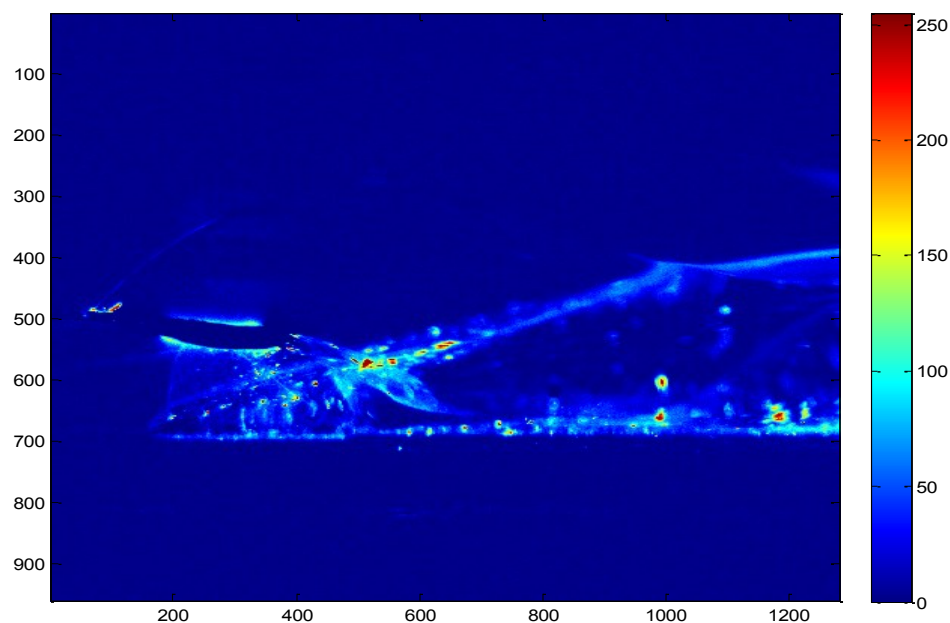


Figure 15. Image taken during injection with drug precipitation

The light intensity values from the image were also used to summarize the in vitro results in a plot vs. time. The region inside the tube, just past the needle tip, was divided into three areas (figure 16) and sampled for an average maximum light intensity value which was plotted for the 60 sequential images taken as a function of time. This sampling method allows us to subtract out sources of light scattering not associated with precipitation such as air bubbles or crystals stuck to the quartz tube. The sampling procedure is also repeated for downstream images with the entire length of the cell being sampled for a light intensity value. The data from these plots will be compared to opacity readings obtained by Johnson (25) using the previously used in vitro device.

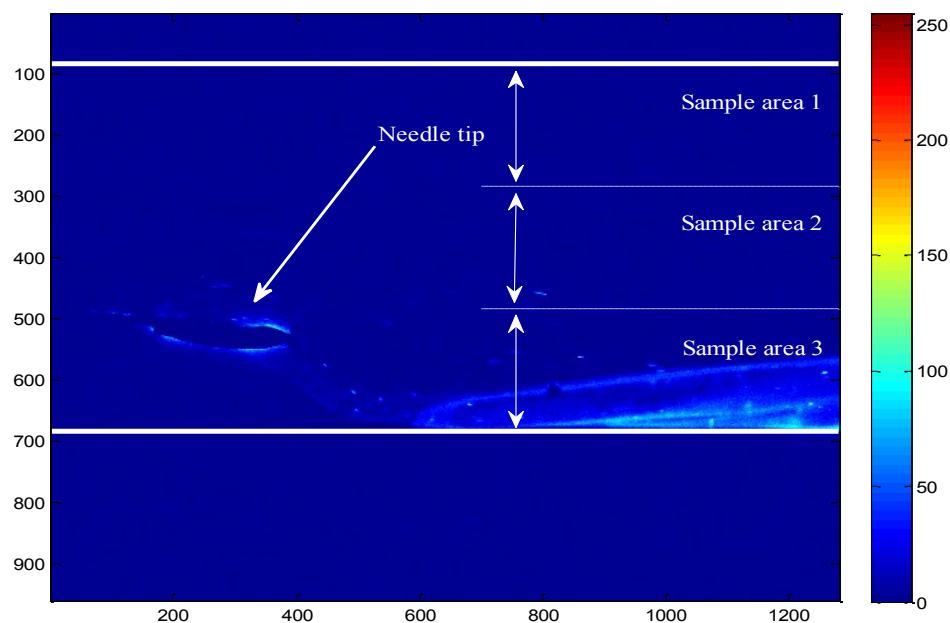


Figure 16. Scaled intensity image after injection of phenytoin sodium

2.2. Computational Software

The new graphical user interface (GUI)- based computational software, shown in figure 17, was created using GUIDE program in Matlab®. The program user enters the drug information and chooses the formulation excipients from a stored list. Users may also create new excipients that will be stored in the excipient data file for future use. After all the information has been entered, the program will predict both the total drug solubility and the effect of blood dilution on the formulation. The program will also allow the user to enter experimental intrinsic and total drug solubility, if available, to improve the accuracy of the calculation. Figure 18 is a comprehensive list of the equations used to estimate the drug solubility and the blood dilution effect.

The screenshot shows the SABDS software interface. It has a title bar with 'SABDS' and standard window controls. The main area is divided into four colored panels: a blue 'FORMULATION' panel, an orange 'INFUSION DILUENT' panel, a green 'USER DEFINED DRUG / EXCIPIENT' panel, and a pink 'BLOOD MODEL' panel. The 'FORMULATION' panel contains a 'Drug' section with a 'Select Drug' button and a table with columns 'Type', 'Name', 'Conc', and 'Units'. Below this is a table with 9 rows labeled 'Excipient 1' through 'Excipient 9'. To the right are 'Adjust Solution' fields for 'Final pH' and 'Final mOsmol/L', and buttons for 'Load Formulation' and 'Clear Data'. The 'INFUSION DILUENT' panel has a checkbox 'Use Infusion Diluent', a dropdown for 'Dextrose 5.00%', and input fields for 'ml of formulation' and 'ml of diluent'. The 'USER DEFINED DRUG / EXCIPIENT' panel has buttons for 'New Drug', 'New Cyclic Peptide', 'New Buffer', 'New Cosolvent', 'New Salt', and 'New Surfactant'. The 'BLOOD MODEL' panel has a table with columns 'Type', 'Name', 'Conc', and 'Units' and 6 rows labeled 'Excipient 1' through 'Excipient 6'. To its right are 'Adjust Solution' fields for 'Final pH' and 'Final mOsmol/L', and buttons for 'Load Blood Model' and 'Clear Data'. At the bottom right are four green buttons: 'Blood Dilution', 'Buffer Capacity', 'Drug Solubility', and 'Export Data'.

Figure 17. Drug solubility and blood dilution program GUI

2.2.1. Computational Results

The computational results will be summarized using the two plots shown in figures 5 and 7. The software will estimate the effect of blood surrogate dilution on the total drug solubility of the formulation and identify potential areas of supersaturation. The results of the calculation will be used to make predictions for the outcomes of in vitro device tests. The chemicalize.org website from Chemaxon (33) was used to calculate log Kow values when consistent literature values were not available.

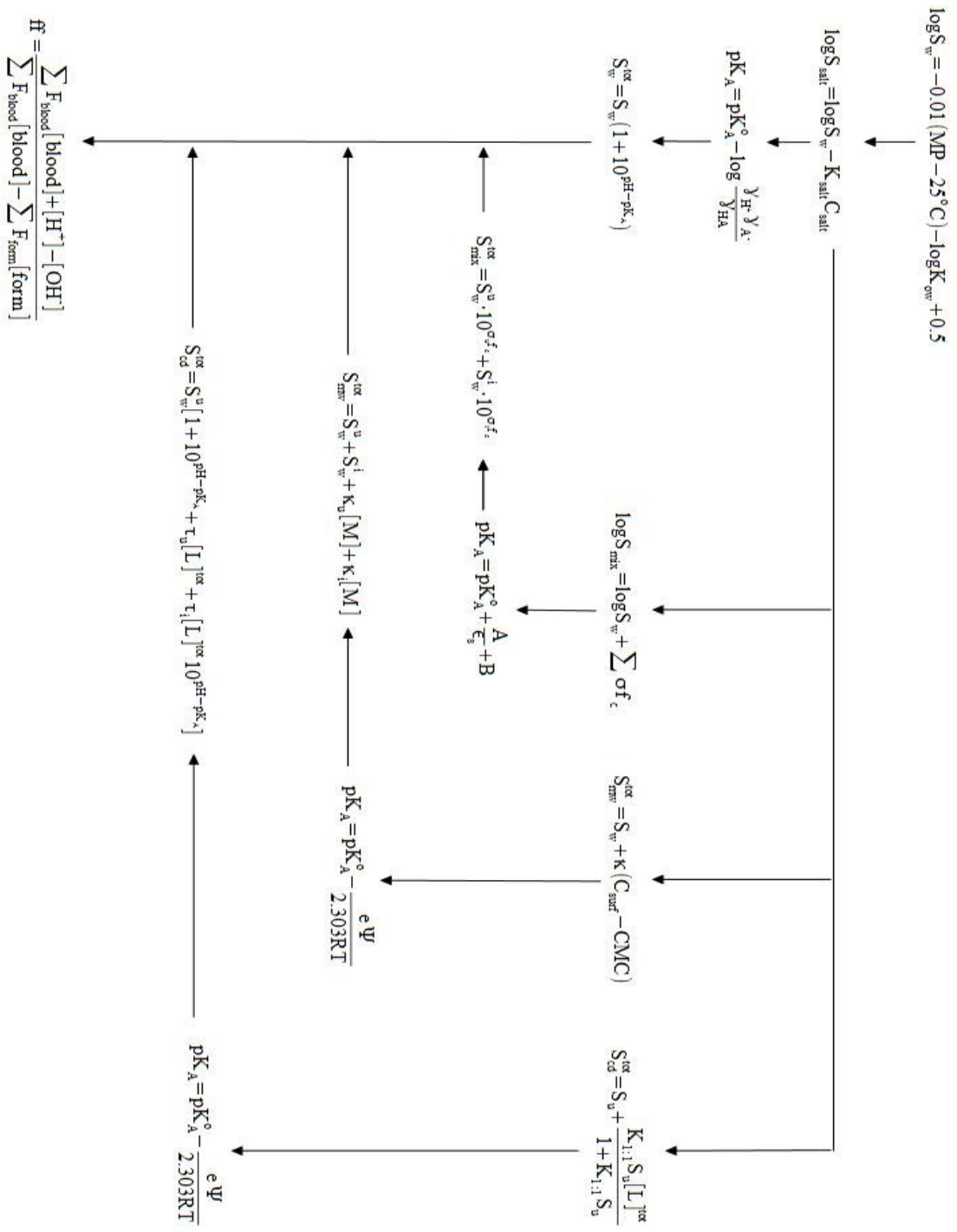


Figure 18. Equations used in the solubility and blood dilution software

2.3. Experiments

2.3.1. Initial Drug Study

Table 2 contains the list of drugs chosen to test the new in vitro device to detect drug precipitation. This list includes information about whether the drug has a significant history of phlebitis reported in literature. Triplicate formulations were made, and pre-diluted if necessary, according to the information provided in the product inserts or in the Handbook of Injectable Drugs (4). ISPB was made according to instructions listed in the Documenta Geigy Scientific Tables (12). Table 14 in the appendix A lists all chemicals used in the study.

Table 2. Drugs Used for In Vitro device study

Drug	↑ Incidence of Phlebitis	Solubilization Method	Manufacturer
Amiodarone HCl	Yes (34)	pH + surfactant	Made from API
Clarithromycin	Some (35)	pH	Made from API
Epinephrine	No (25)	pH	Made from API
Furosemide	No (25)	pH	Made from API
Phenytoin Sodium	Yes (36)	pH + Cosolvent	Made from API
Verapamil HCl	Yes (37)	pH	Made from API
Proprietary Form 1	Yes*	pH	Made from API
Proprietary Form 2	No*	pH	Made from API
Proprietary Form 3	No*	pH	Made from API
*Personal communication from pharmaceutical company			

All formulations were filtered with a 0.45µm PTFE Acrodisc® syringe filter prior to injection and ISPB was filtered with 0.45 µm Nalgene® nylon filter system. With the exception of the proprietary antibiotic formulations, both active (excipients + drug) and

placebo (excipients) formulations were injected at 1 and 5 ml/min into the flowing (5ml/min) ISPB blood surrogate ($T=25\pm1.7^{\circ}\text{C}$). The injection rate used for the proprietary antibiotic formulations were 4ml/min, which is the infusion rate specified by the pharmaceutical company.

2.3.2. Temperature Study

The isotonic phosphate buffer was chosen as the blood surrogate because it has the same buffering capacity of 38mEq/L **(38)** (figure 19) and osmolarity (308mOsmol/L **(12)**) of human blood. There have been other published in vitro studies where the author attempted to more closely model blood by raising the phosphate blood surrogate temperature to 37°C **(39)**.

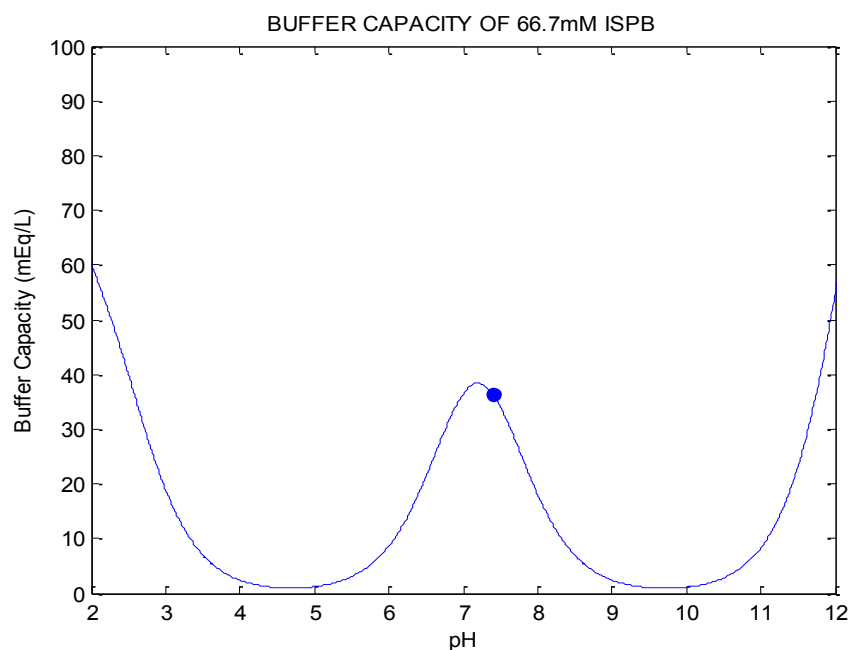


Figure 19. Buffer capacity of ISPB

Temperature may factor into drug precipitation because the aqueous solubility of most drug solutes will increase as the solution temperature increases. Therefore, a study was done to determine if increasing the temperature of the blood surrogate to match the blood temperature in the body would change the results of the in vitro device. To simulate the temperature of blood in the body the isotonic phosphate buffer was placed inside a Quincy 12-140E incubator set for $37 \pm 0.7^{\circ}\text{C}$ overnight. Prior to injection the temperature of the phosphate buffer was confirmed with a Fisher Scientific infrared thermometer gun. The drugs chosen for this study are listed in table 3. Active (drug + excipients) and placebo (excipients) formulations were injected at 1 ml/min into the flowing ISPB blood surrogate for one minute total. During the temperature study, images were taken only at the needle tip at one second intervals for the one minute injection.

Table 3. Drugs Used for In Vitro temperature and serum albumin study

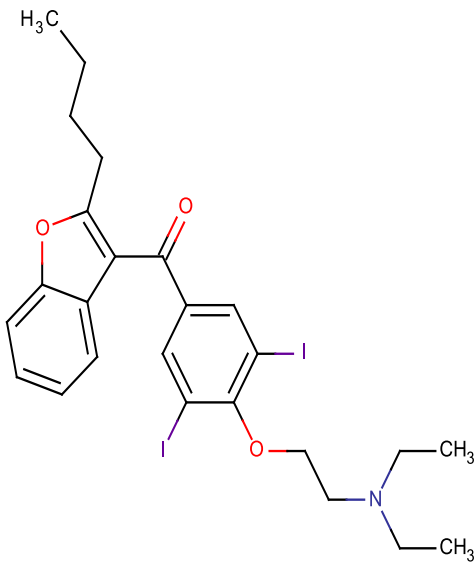
Drug	Incidence of Phlebitis	Solubilization Method
Amiodarone HCl	Yes	pH + surfactant
Phenytoin Sodium	Yes	pH + Cosolvent
Verapamil HCl	Yes	pH

CHAPTER 3: RESULTS AND DISCUSSION

3.1. Initial Drug Study Results

3.1.1. Amiodarone Hydrochloride

Amiodarone Hydrochloride is an antiarrhythmic agent approved in the US to treat life-threatening ventricular arrhythmias (**40**). The chemical structure of amiodarone is shown in table 4 along with the important physical properties used in our calculation.

Table 4. Physical properties and chemical structure of amiodarone													
<table border="1"> <thead> <tr> <th>Property</th><th>Value</th></tr> </thead> <tbody> <tr> <td>Melting Point</td><td>159⁰C (41)</td></tr> <tr> <td>C log K_{ow} (neutral)</td><td>7.64 (33)</td></tr> <tr> <td>C log K_{ow} (ionized)</td><td>4.13 (33)</td></tr> <tr> <td>log Sw</td><td><-2.5 uM (42)</td></tr> <tr> <td>pKa</td><td>8.7 (42)</td></tr> </tbody> </table>	Property	Value	Melting Point	159 ⁰ C (41)	C log K _{ow} (neutral)	7.64 (33)	C log K _{ow} (ionized)	4.13 (33)	log Sw	<-2.5 uM (42)	pKa	8.7 (42)	
Property	Value												
Melting Point	159 ⁰ C (41)												
C log K _{ow} (neutral)	7.64 (33)												
C log K _{ow} (ionized)	4.13 (33)												
log Sw	<-2.5 uM (42)												
pKa	8.7 (42)												

To overcome its low intrinsic aqueous solubility, amiodarone is formulated as the hydrochloride salt with a pH between 3 and 3.5 and uses 100 mg/ml of polysorbate 80 and 20.2 mg/ml of benzyl alcohol to reach the final concentration of 50 mg/ml. Before injection the concentrated drug formulation is then diluted with dextrose 5% to a final concentration of 1.5 mg/ml with the pH remaining roughly the same. Ignoring the diluted

benzyl alcohol (0.058%), the total aqueous solubility of a formulation using pH control and surfactant can be estimated using the following equation (6):

$$S_{mw}^{tot} = S_w [(1 + K_{mu}) + (1 + K_{mi}) 10^{pK_a - pH}] \quad (15)$$

Where K_{mu} and K_{mi} are the micellar-water partition coefficients (for the unionized and ionized drug respectively) which can be estimated for polysorbate 80 using the drug's log K_{ow} and the following relationship (43).

$$\log K_{mw} = 0.9201 \log K_{ow} + 0.0690 \quad (16)$$

3.1.1.1. Software Results

Figure 20 shows the experimental (solid line) and theoretical (dashed line) pH solubility plot for amiodarone hydrochloride recreated from Bergstrom et al (42). Due to the self-association of amiodarone, the increase in solubility between pH 7.4 and 5 is much greater than predicted by equation 2. Figure 21 is a plot of the amiodarone formulation pH vs the fraction of formulation obtained by the blood dilution simulation software. This plot predicts that the pH of the unbuffered amiodarone formulation will increase rapidly from 3.5 to 7.4 upon mixing with the blood surrogate. According to figure 22 this rapid rise in pH, along with the dilution of remaining surfactant, will result in the solubility curve dropping below the concentration line forming a transient supersaturated solution. A conclusion from the dilution calculation is that there is the possibility that the amiodarone HCl formulation will precipitate upon dilution with blood surrogate.

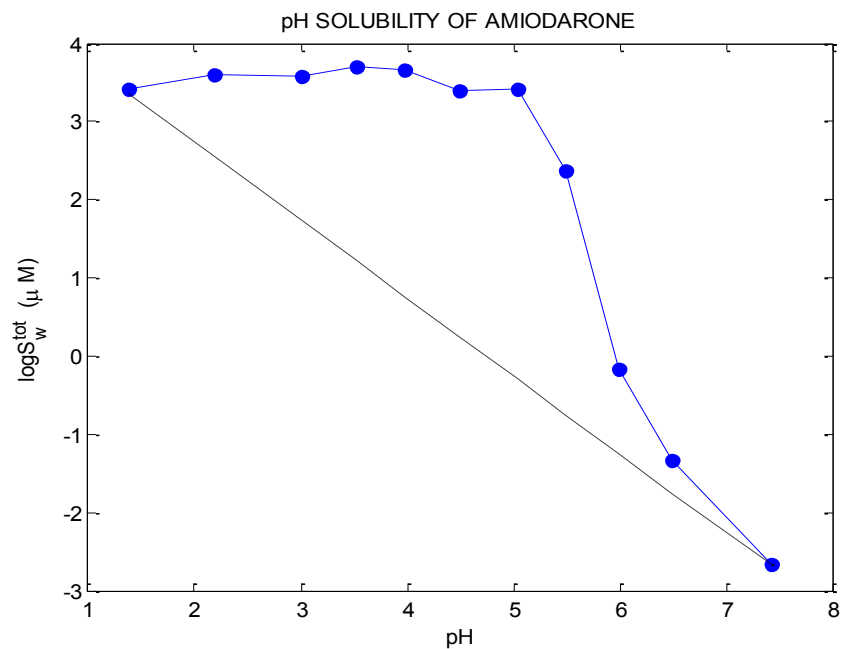


Figure 20. pH-solubility curve for amiodarone

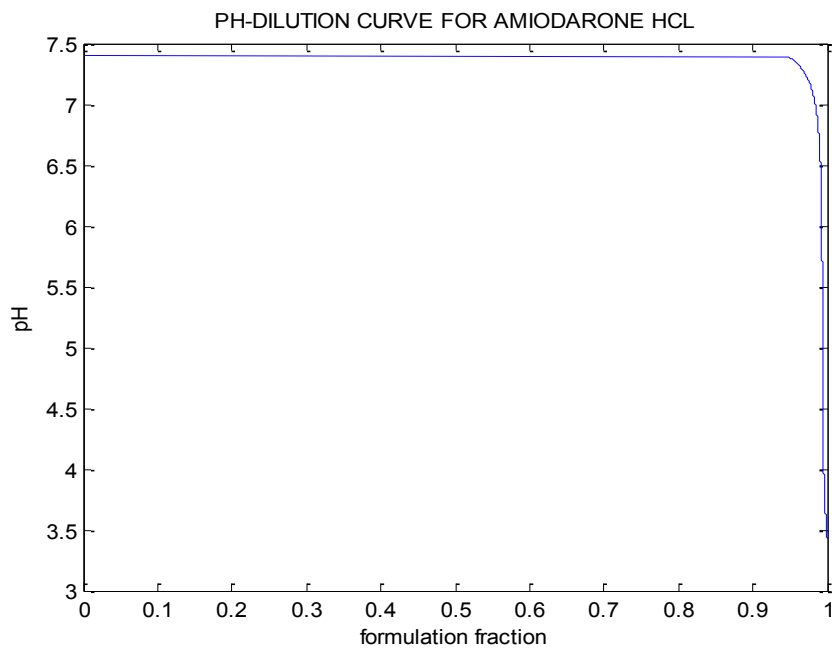


Figure 21. pH-dilution curve for amiodarone HCL

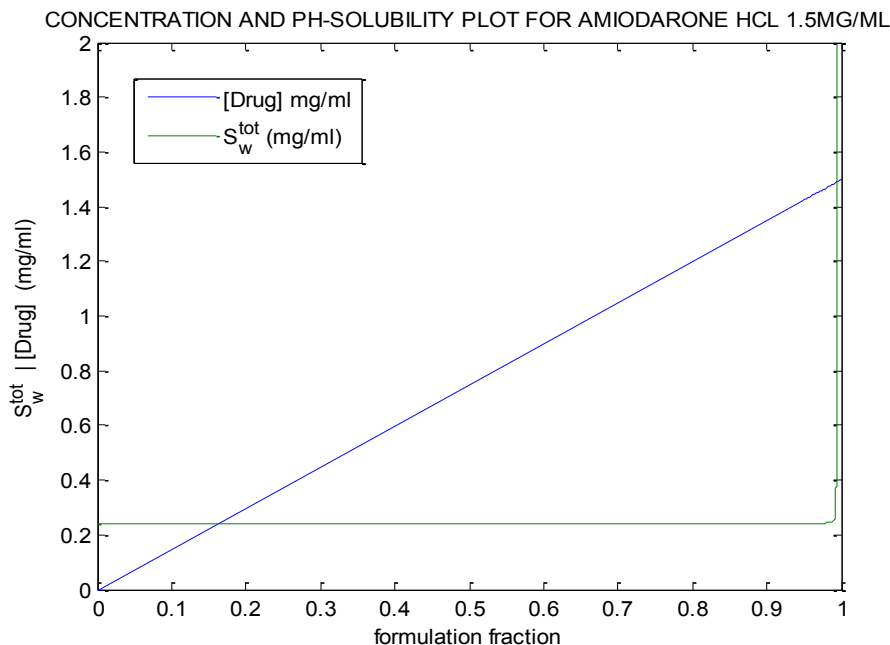


Figure 22. Drug concentration and solubility plot for amiodarone HCl

3.1.1.2. In Vitro Results

Figure 23 is a plot of light intensity vs. time and shows that the amiodarone formulation does precipitate upon mixing with ISPB blood surrogate at both rates and detector locations. While all samples precipitated to some degree, figure 23 indicates that the precipitation was higher both downstream from the needle tip and at lower injection rates. This increase in precipitation at the lower injection rate seems to contradict those obtained by Johnson (25) where the 5 ml/min injection rate had a higher opacity reading (0.32) than the 1ml/min injection rate (0.24). However, the earlier in vitro device had approximately 40cm of tubing separating the point of injection and the detector, while in this study the detector was never farther than 10 centimeters from the needle tip. This longer distance presumably gave the formulation enough time to mix with the blood

surrogate and produce more precipitation. The increase in precipitation that occurs downstream of the needle tip for both injection rates in our study makes this explanation more plausible.

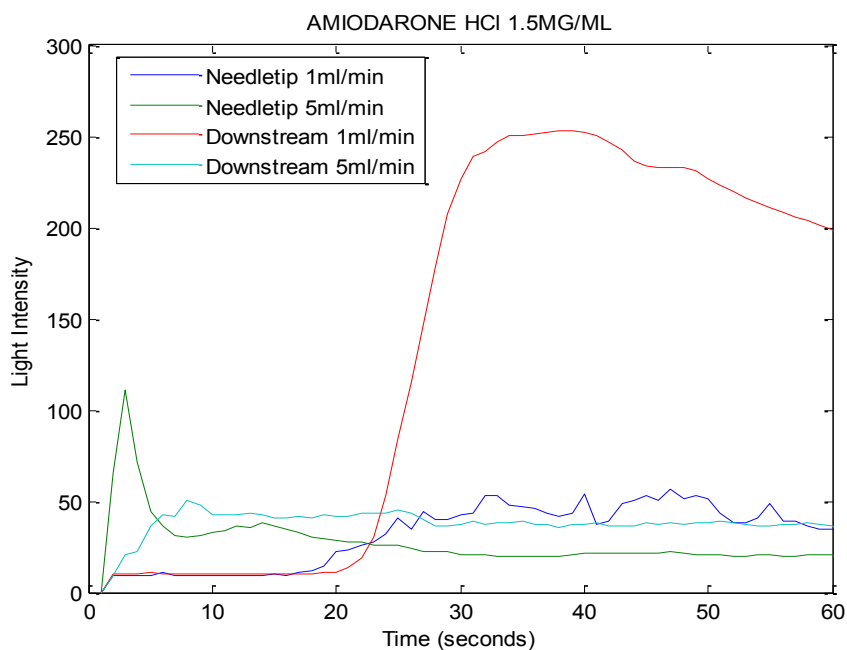


Figure 23. In vitro results for amiodarone HCl

Figure 23 is the scaled intensity image for the placebo formulation during the 1ml/min injection at the needle tip. Figure 24 is the intensity image of the flow cell near the needle tip during the 1ml/min injection of the formulation containing the active drug.

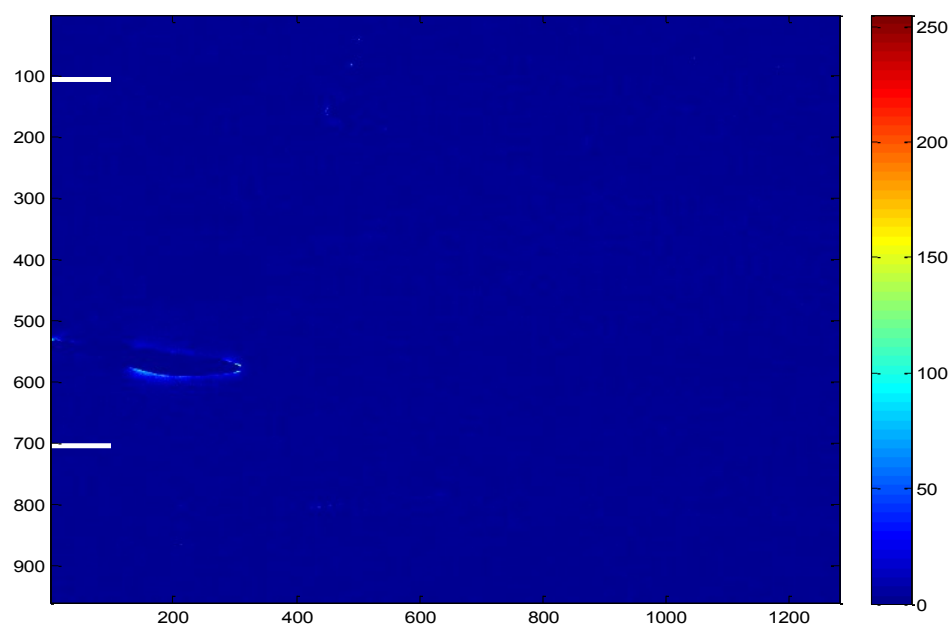


Figure 24. Image of the needle tip during the 1ml/min placebo amiodarone injection

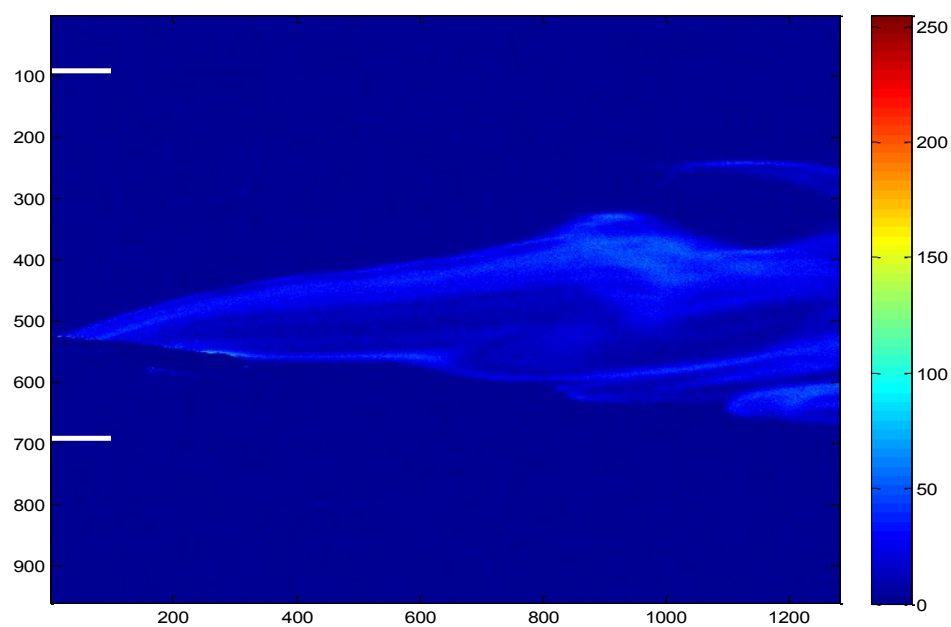


Figure 25. Image of the needle tip during the 1ml/min active amiodarone injection

The downstream image of the 1ml/min injection (figure 26) shows the higher amount of precipitation at the lower injection rate tends to stay towards the bottom of the flow cell presumably due to gravity effects. For the higher injection speed (figure 26) there is a lower amount of precipitation which is more uniformly spread throughout the cell due to the increased overall flow rate through the tube. The amiodarone formulation that was tested has a high incidence of phlebitis reported in the literature (34) (44). It seems likely that the drug precipitating at the needle tip is the cause of this pain felt after injection.

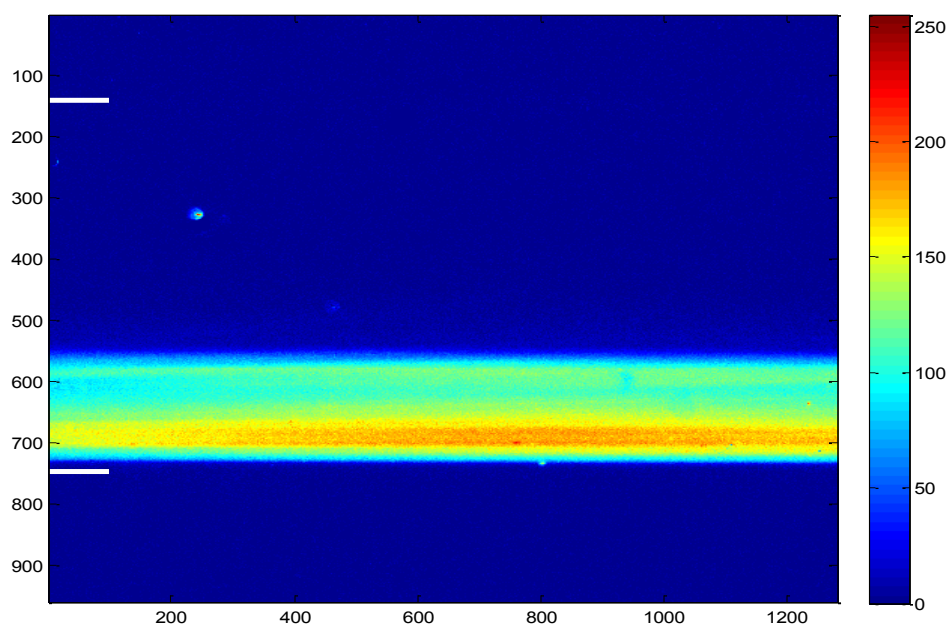


Figure 26. Image of the 1ml/min amiodarone injection downstream

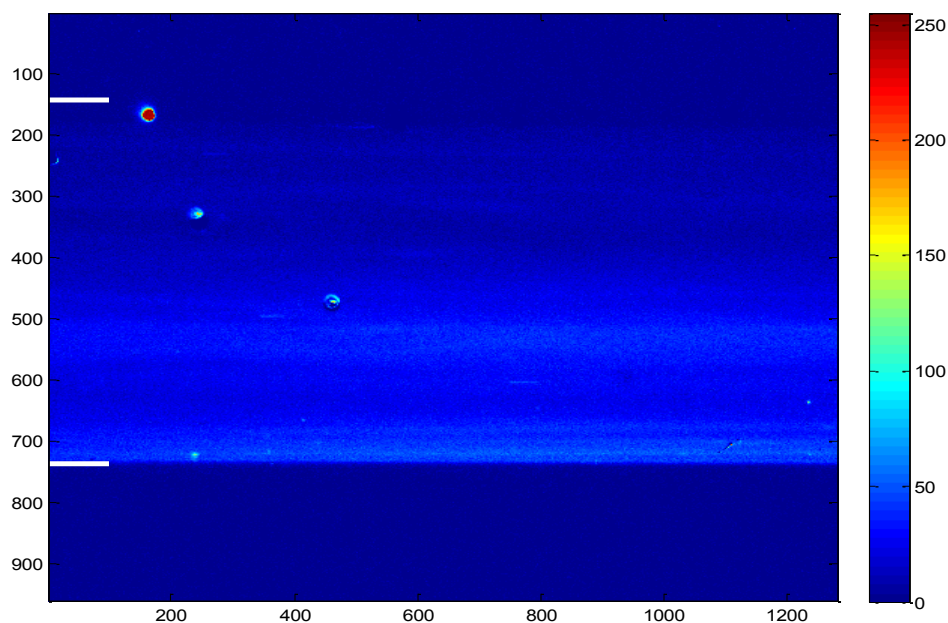
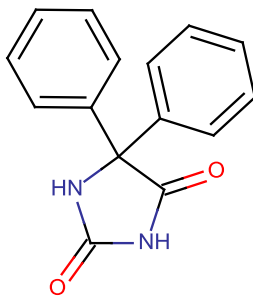


Figure 27. Image of the 5ml/min amiodarone injection downstream

3.1.2. Phenytoin Sodium

Phenytoin, or 5,5-diphenylhydantoin, is an FDA approved drug for the treatment of epileptic seizures (45). The chemical structure of phenytoin is shown in table 5 along with a list of important physical properties, some of which are used in our dilution calculation. The IV formulation of phenytoin contains its sodium salt (50mg/ml) at pH 12 in a solution consisting of 10% ethanol and 40 % propylene glycol. This IV formulation has perhaps the highest incidence of phlebitis recorded in the literature, rivaled only by the IV formulation of diazepam (Valium). Interestingly, these two formulations were actually prescribed together and contain the same cosolvents in the same quantities (46).

Table 5. Physical properties and chemical structure of phenytoin

Property	Value	
Melting Point	297.1 ⁰ C (47)	
C log K _{ow} (neutral)	2.15 (33)	
C log K _{ow} (ionized)	0.20 (33)	
log Sw	-4.13M (48)	
pKa	8.06 (48)	

The solubility of a drug using both pH control and cosolvents can be estimated by (6):

$$S_{\text{mix}}^{\text{tot}} = S_w (10^{\sum \sigma_u f_c} + 10^{\text{pH}-\text{pKa}} 10^{\sum \sigma_i f_c}) \quad (17)$$

Where σ_u and σ_i are the solubilization slopes for the unionized and ionized drug respectively. To estimate the total drug solubility, the σ_u value for phenytoin was obtained from the literature (6), and the σ_i value was estimated from the logK_{ow} of the ionized drug using the following empirical relationships for slope estimation (49).

$$\sigma_{\text{etoh}} = 0.903 \log K_{\text{ow}} + 0.402 \quad (18)$$

$$\sigma_{\text{pg}} = 0.57 \log K_{\text{ow}} + 0.38 \quad (19)$$

3.1.2.1. Software Results

The pH solubility curve for phenytoin for both 25⁰C, (48) and 37⁰C (50) are shown in figure 28. The 37⁰C plot was included because it shows the decrease in solubility when the K_{sp} is exceeded for the sodium salt around pH 12. Because phenytoin sodium is unbuffered, a sharp decrease in the pH upon dilution with blood might be initially

expected. However, due to the total drug (182.3mM), and sodium hydroxide concentrations relative to the sodium phosphate buffer (67mM), the drop in pH as a function of formulation fraction is almost linear (figure 29). While the pH does not decrease as rapidly as it did for the amiodarone formulation during our dilution simulation, the solubility decrease was still rapid enough to fall below the concentration which resulted in a supersaturated solution (figure 30). Thus, the dilution software predicts that the phenytoin sodium 50mg/ml formulation has the potential to precipitate upon dilution with the ISPB blood surrogate.

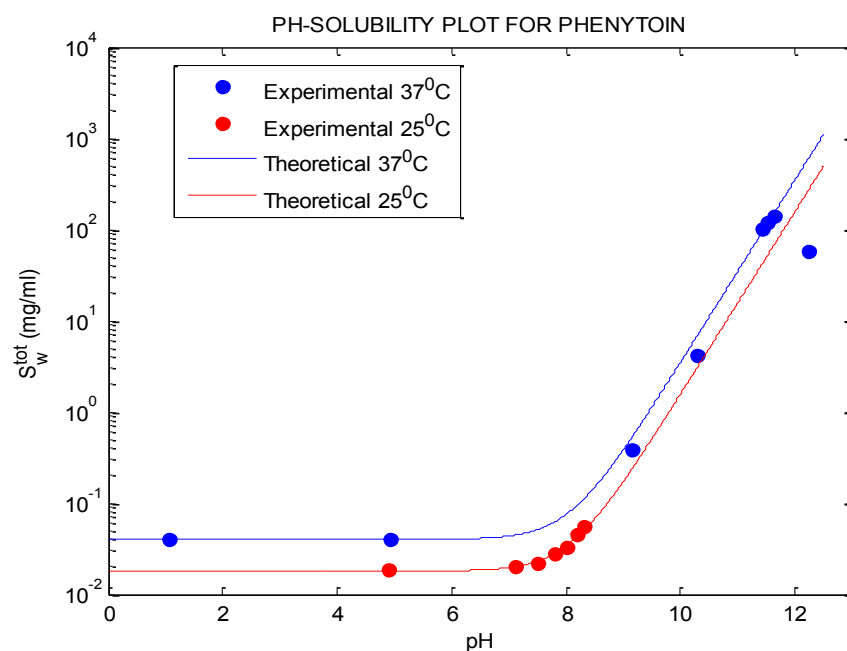


Figure 28. pH-solubility plot for phenytoin

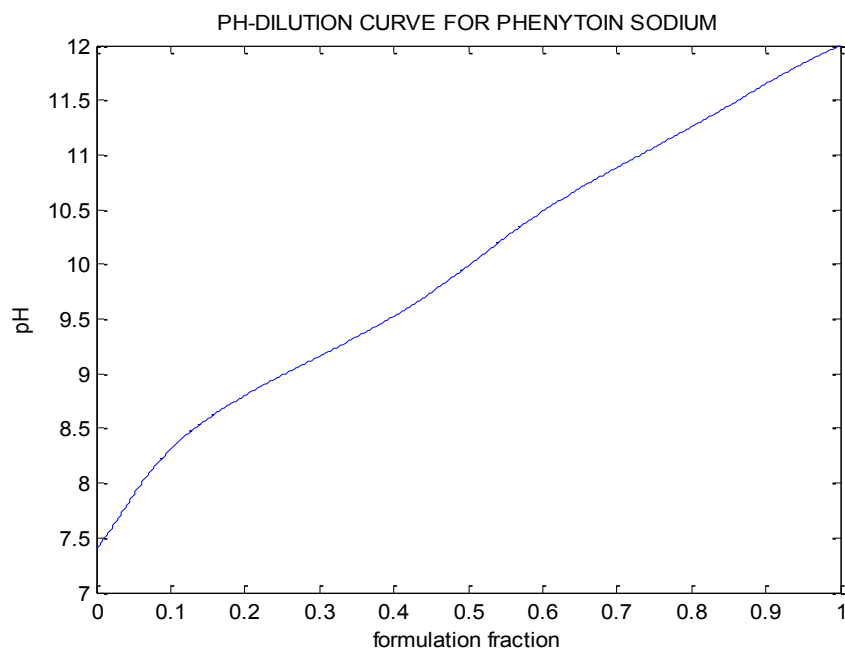


Figure 29. pH-dilution curve for phenytoin sodium

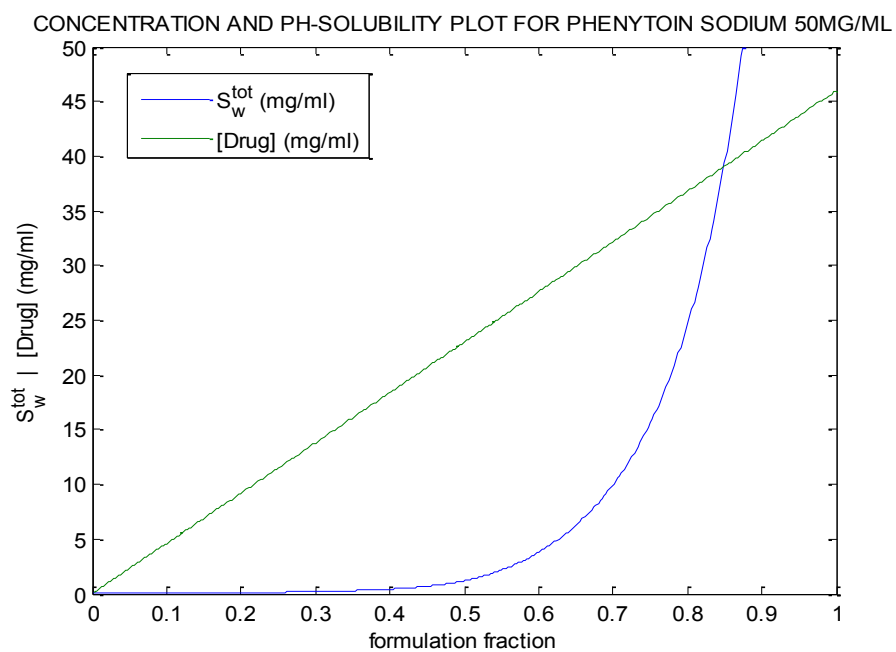


Figure 30. Drug concentration and solubility plot for phenytoin sodium

3.1.2.2. In Vitro Results

The in vitro results, summarized in the plot of light intensity vs. time in figure 31, for phenytoin sodium show a large amount of drug precipitation both at the needle tip and downstream for all injection rates. This precipitation included needle shaped crystals and aggregates of needle shaped crystals which are best visualized using an image taken at an injection rate of 0.5 ml/min (figure 32). In the 1ml/min injection phenytoin sodium produced more precipitation at the needle tip than downstream while the 5ml/min injections were both close to the maximum value. Using the earlier device, Johnson (25) found that the amount of drug precipitation actually decreased with increasing injection rate due to a phenomenon referred to as “plug flow”. This “plug flow” describes the rapid injection moving down the tubing as a plug with only the edges of the formulation being exposed to the phosphate buffer where precipitation can occur. The quartz tube has a wider diameter (4mm) than the tubing used in the earlier study (3mm) and along with the different flow cell design may account for us not seeing this “plug flow” event. The scaled intensity image of the 1ml/min injection (Figure 33) shows the high amount of precipitation at the needle tip as the formulation is pushed out of the tube. Figure 33 is the image downstream of the needle tip at during the 1ml/min injection showing the precipitation. This precipitation stays towards the bottom of the flow cell because the formulation contains the higher density cosolvent propylene glycol.

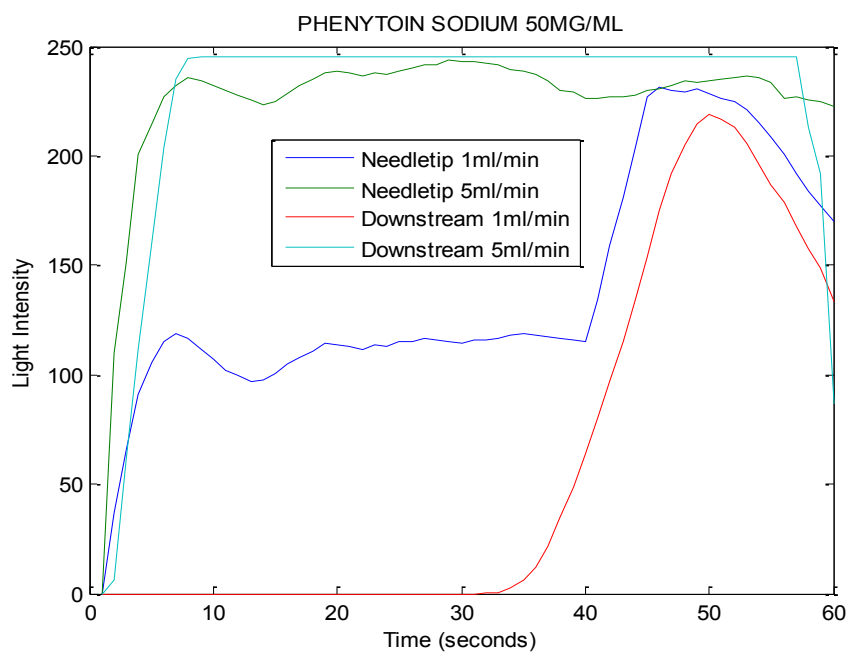


Figure 31. In vitro results for phenytoin sodium 50 mg/ml

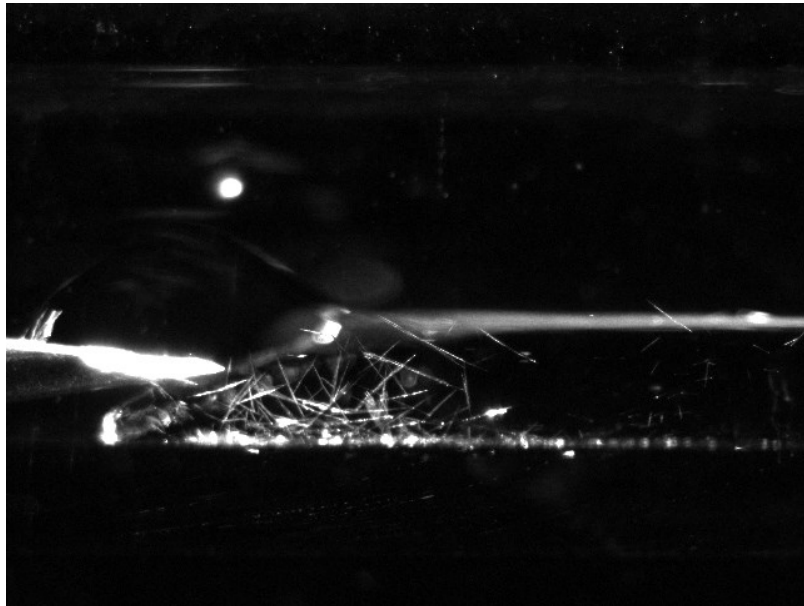


Figure 32. Image of needle tip during a 0.5 ml/min injection of phenytoin sodium

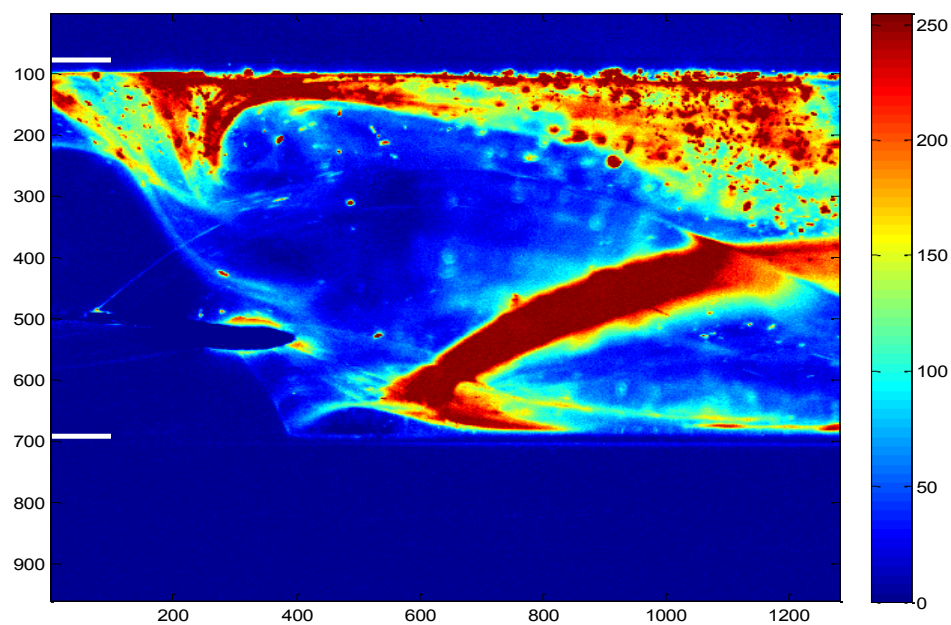


Figure 33. Image of the needle tip during the 1ml/min phenytoin sodium injection

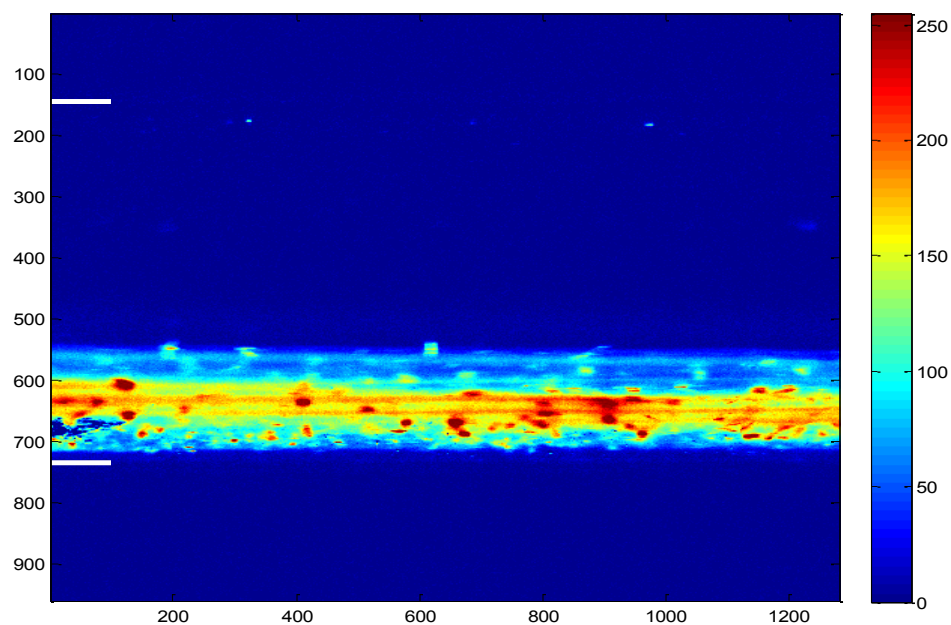


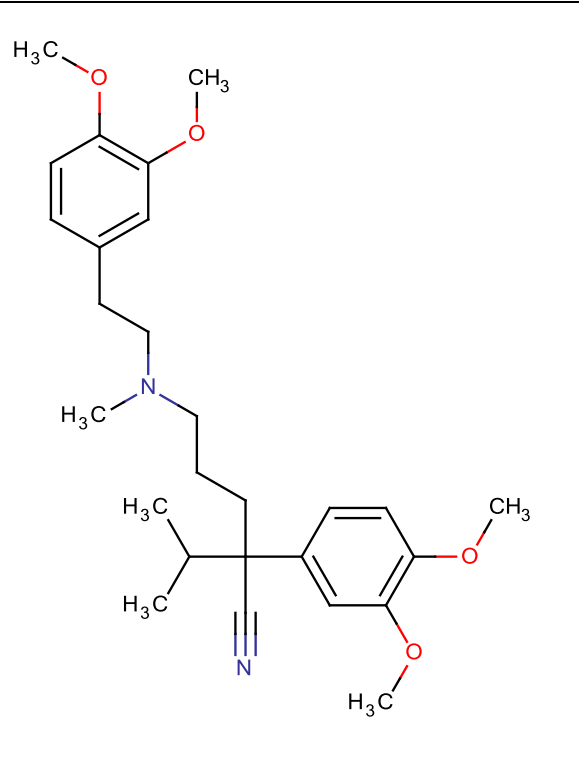
Figure 34. Downstream image of the 1ml/min phenytoin sodium injection

3.1.3. Verapamil HCl

Verapamil HCl is an antiarrhythmic drug used in the treatment of atrial tachyarrhythmias and angina (**51**). The chemical structure of verapamil is shown in table 6 along with a list of important physical properties, some of which are used in our dilution calculation.

The IV formulation contains 2.5mg/ml of the hydrochloride salt of verapamil at pH 4.9 and 8.5 mg/ml of sodium chloride.

Table 6. Physical properties and chemical structure of verapamil

<table> <tr> <th>Property</th><th>Value</th></tr> <tr> <td>Melting Point</td><td>146 °C (52)</td></tr> <tr> <td>log K_{ow}</td><td>4.6 (42)</td></tr> <tr> <td>log S_w</td><td>-3.97 M (53)</td></tr> <tr> <td>pKa</td><td>9.1 (42)</td></tr> </table>	Property	Value	Melting Point	146 °C (52)	log K _{ow}	4.6 (42)	log S _w	-3.97 M (53)	pKa	9.1 (42)	
Property	Value										
Melting Point	146 °C (52)										
log K _{ow}	4.6 (42)										
log S _w	-3.97 M (53)										
pKa	9.1 (42)										

3.1.3.1. Software Results

Figure 35 shows the experimental and theoretical pH-solubility plot for verapamil (42). When the unbuffered verapamil HCl formulation is titrated with blood surrogate in the dilution calculation, the pH rapidly rises from pH 4.9 to pH 7.4 (figure 36). This rapid increase in the formulation pH causes the solubility to drop below the formulation concentration during the dilution simulation and results in a supersaturated solution (figure 37).

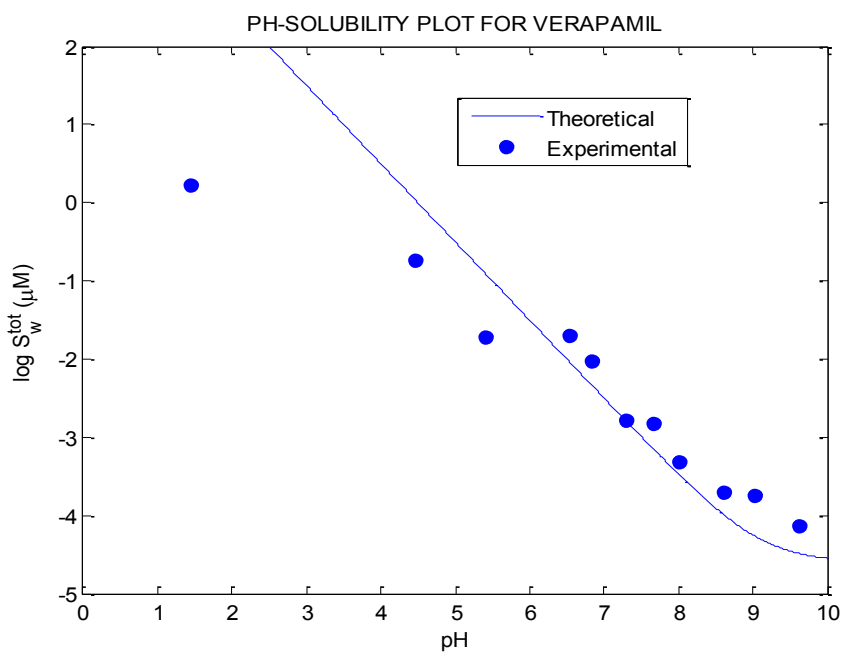


Figure 35. pH solubility plot for verapamil

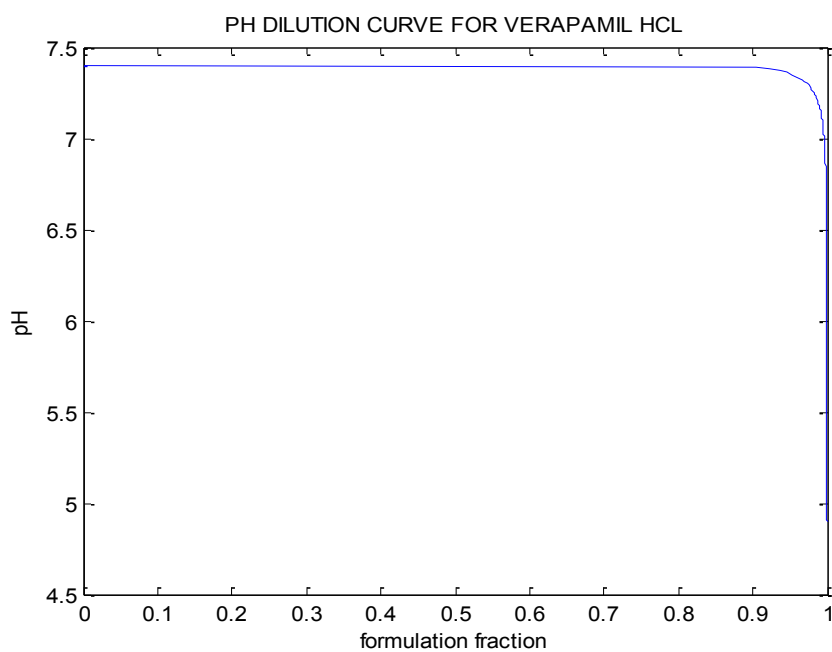


Figure 36. pH-dilution curve for verapamil HCl

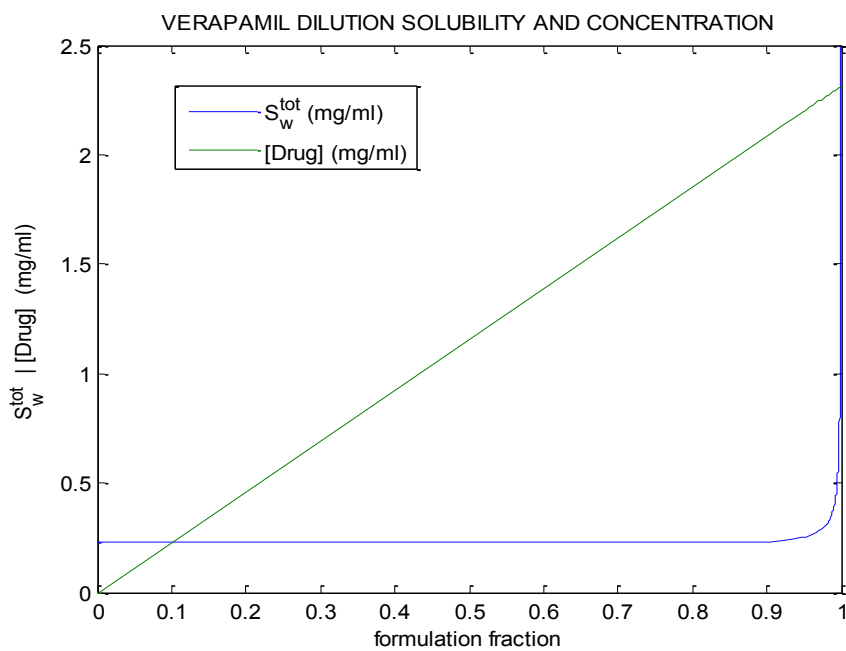


Figure 37. Drug concentration and solubility plot for verapamil HCl

3.1.3.2. In Vitro Results

The in vitro results summarized in figure 38 shows that verapamil HCl does precipitate upon dilution with ISPB blood surrogate. This precipitation becomes more significant as the formulation moves downstream and also at higher injection rates. Figure 39 is the image of the needle tip during the 5 ml/min injection using a smaller scale to more easily view the precipitation. Figures 40 and 41 are the images downstream of the needle tip where the precipitation of verapamil HCl is higher. This precipitation stays towards the top of the tube because the verapamil formulation contains no high density excipients such as cosolvents or surfactants.

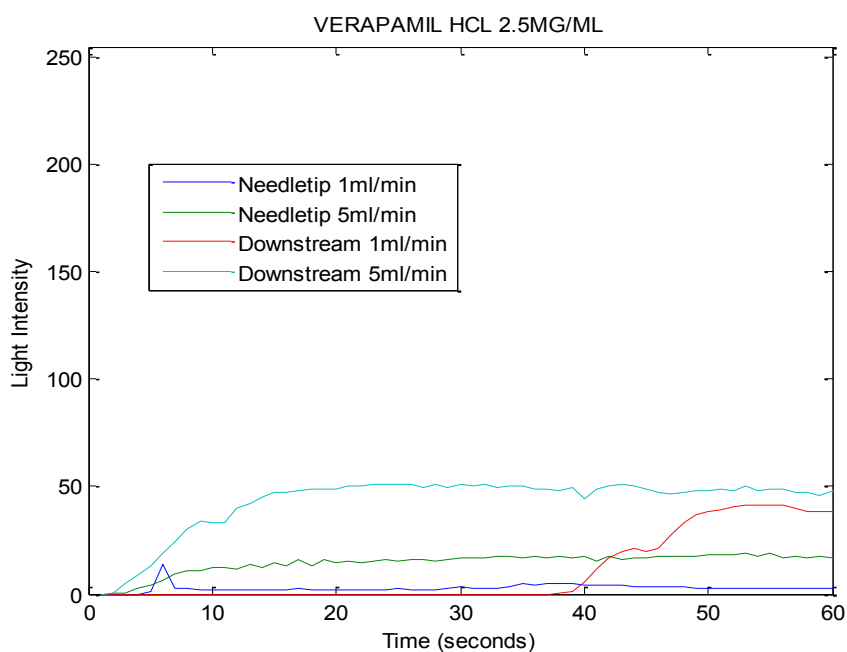


Figure 38. In vitro results for verapamil HCl.

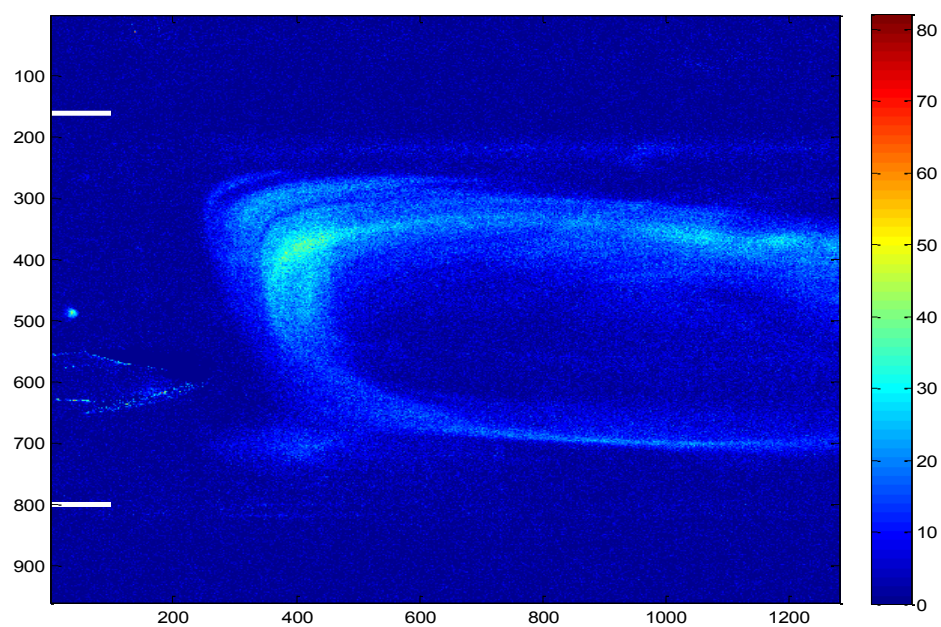


Figure 39. Image of needle tip for 1ml/min verapamil HCl injection

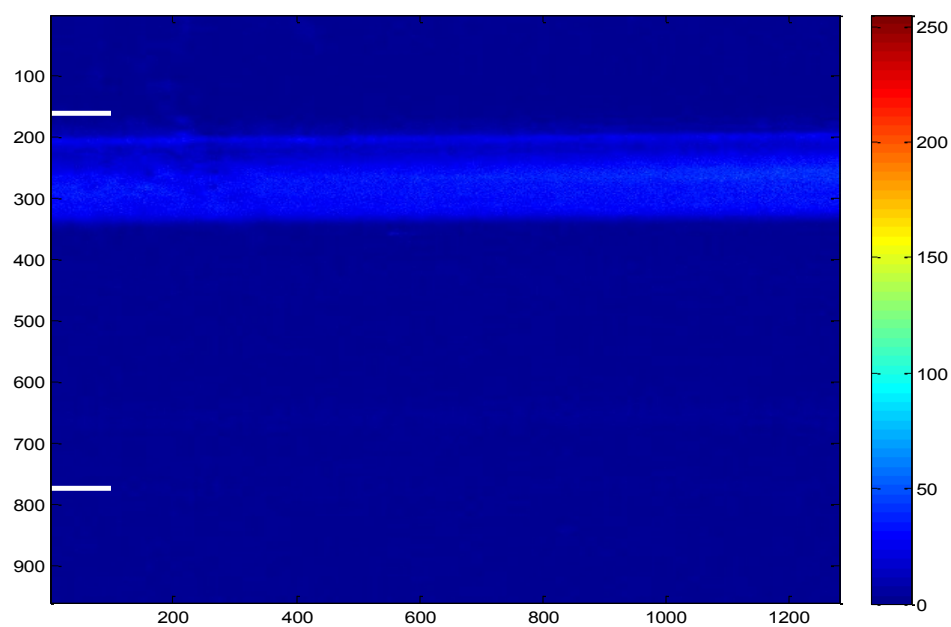


Figure 40. Image of 1ml/min verapamil HCl injection downstream

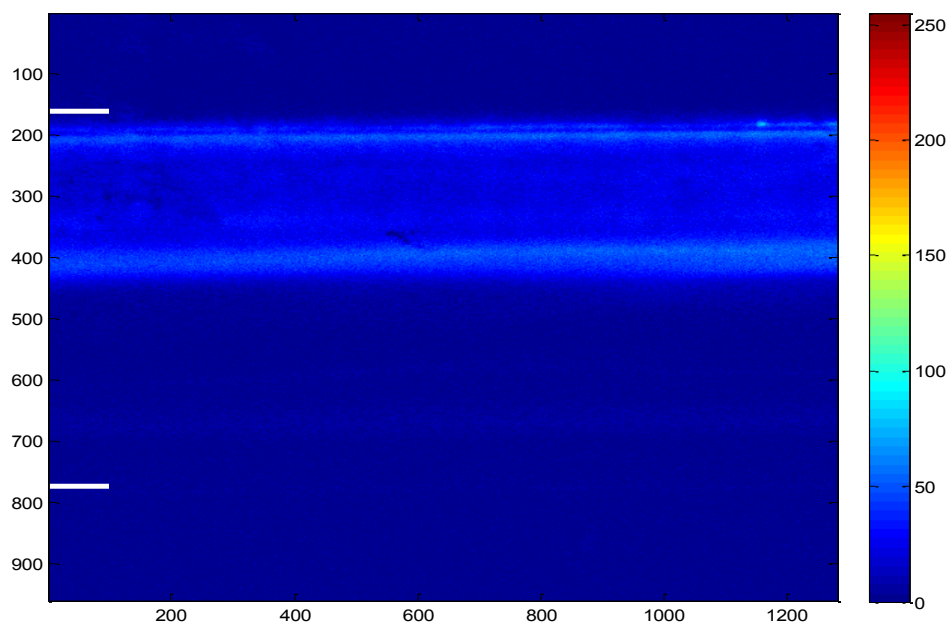


Figure 41. Image of 5ml/min verapamil HCl injection downstream

3.1.4. Proprietary Antibiotic

The proprietary macrolide antibiotic used in the in vitro study is currently undergoing clinical trials for the treatment of various types of infections. The structure of erythromycin, which has a similar macro lactone ring, is shown in table 7 along with the proprietary antibiotic's physical properties. The original formulation contained the active pharmaceutical ingredient, or API (50 mg/ml), tartaric acid (5.8 mg/ml), mannitol (50 mg/ml), and enough sodium hydroxide to bring the pH up to 4.0. This formulation was to be diluted to a concentration of 2mg/ml with 0.9% sodium chloride (Prop1) and infused at injection rates of 1-6ml/min.

Table 7. Physical properties of the proprietary antibiotic and chemical structure of erythromycin

Property	Value
Melting Point	244*
log K _{ow} (est)	5.76 (33)
log S _w (est)	-6.33M**
pKa (exp)	3.5, 9.44*
* Personal communication with company ** Estimated from Henderson-Hasselbalch	

To reduce the chance of drug precipitation upon dilution with blood, two additional formulations, listed in table 8, were developed each containing a small amount of buffering agent.

Table 8. Buffers used in proprietary antibiotic formulations

Form ID	Drug Conc	Buffers	pH
Prop1	2mg/ml	Tartaric Acid (1.5mM)	4.0
Prop2	2mg/ml	Lactic Acid (50mM)	4.0
Prop3	2mg/ml	Histidine (15mM) + Glutamic Acid (15mM) + Aspartic Acid (15mM)	4.5

3.1.4.1. Software Results

Figure 42 shows the estimated pH-solubility plot for the proprietary antibiotic (PA) based on experimental data. Because the solubility drops from an estimated 315 mg/ml to 0.09 mg/ml as the pH increases from 4.0 to 7.4, the buffer capacity of the formulation is

important in determining whether or not the drug will precipitate upon dilution. In addition to buffering capacity, it was discovered that the low solubility product of the citrate and tartrate salts of the PA prevented these buffers from being used. The PA also precipitated out of solution when mixed with the negatively charged sulfobutylether-beta-cyclodextrin.

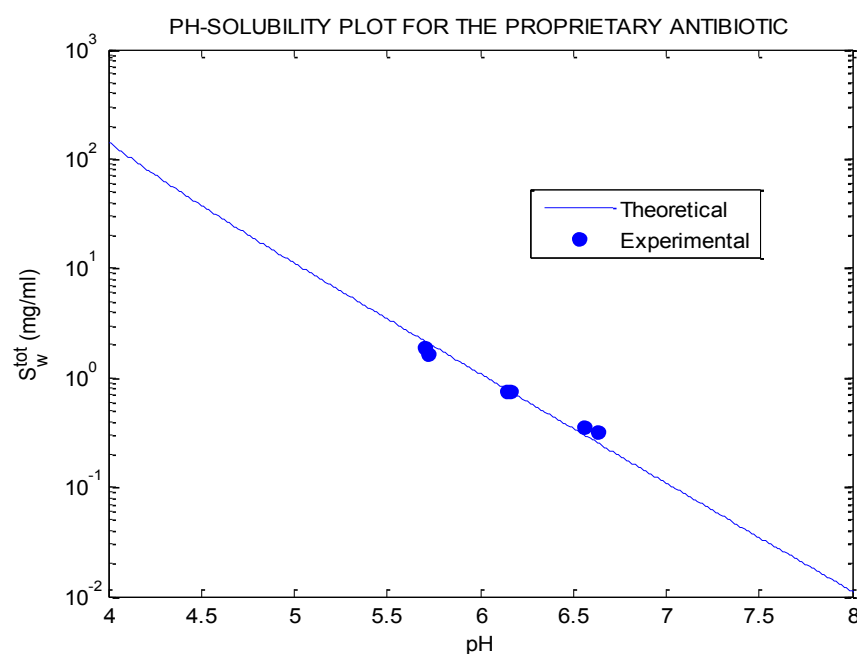


Figure 42. pH-solubility plot for the proprietary antibiotic

Figures 43 and 44 show the buffer capacity and pH dilution curve for the three formulations tested in this study respectively. The initial drug formulation containing 1.5mM of tartaric acid ($pK_{a1}=2.89$, $pK_{a2}=4.40$) has virtually no buffering capacity and quickly rises from 4 to pH 7 upon dilution. The second formulation containing 50mM of lactic acid ($pK_a=3.86$) has approximately 6 times the buffering capacity of the initial formulation at pH 4 and has a much lower formulation fraction at pH 7. The formulation

containing 15mM Histidine ($pK_{a2}=6.10$), 15mM Aspartic Acid ($pK_{a2}=3.77$), and 15mM Glutamic Acid ($pK_{a2}=4.15$) has a similar buffering capacity and pH-dilution profile between pH 4.5 and 7.4 as the lactic acid formulation between pHs 4 and 7.4. The last plot (figure 45) shows that the lactic acid ($AUC=0.4391$) and tri-amino buffer (0.4946) formulations both have lower areas of supersaturation than the initial formulation ($AUC=0.8478$). It is important to reiterate that this lower area of supersaturation reduces the probability that the drug will precipitate upon dilution.

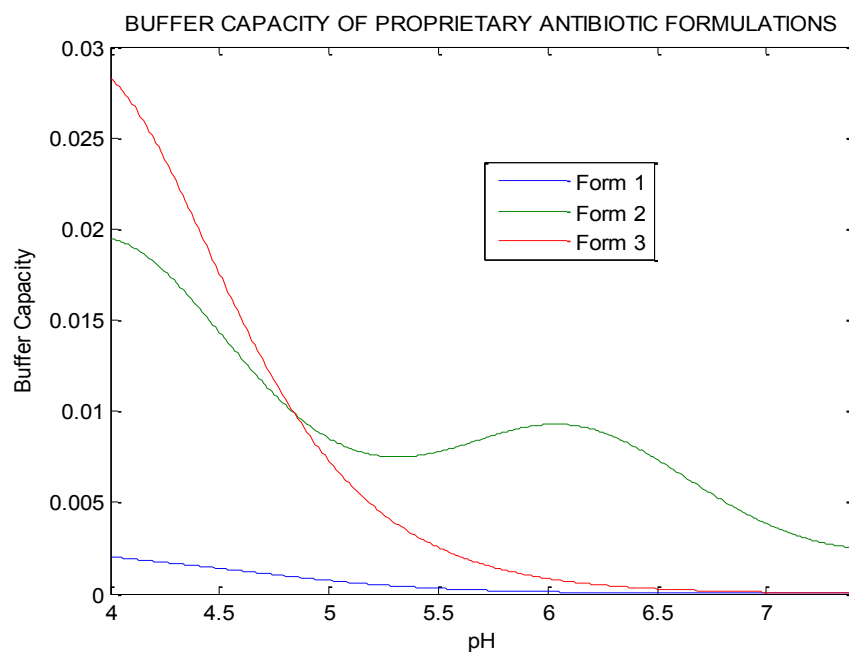


Figure 43. Buffer capacity of proprietary antibiotic formulations

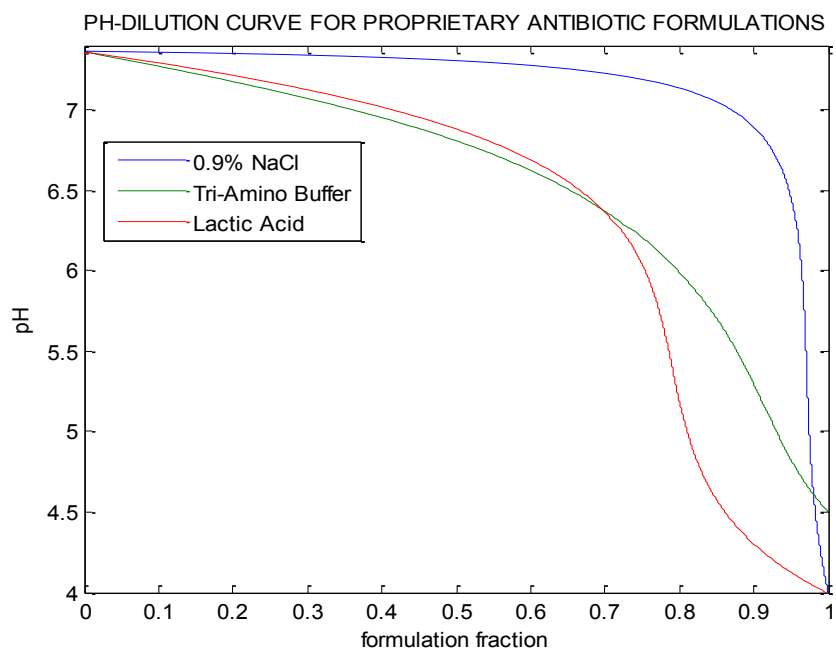


Figure 44. pH-dilution curve for proprietary antibiotic formulations

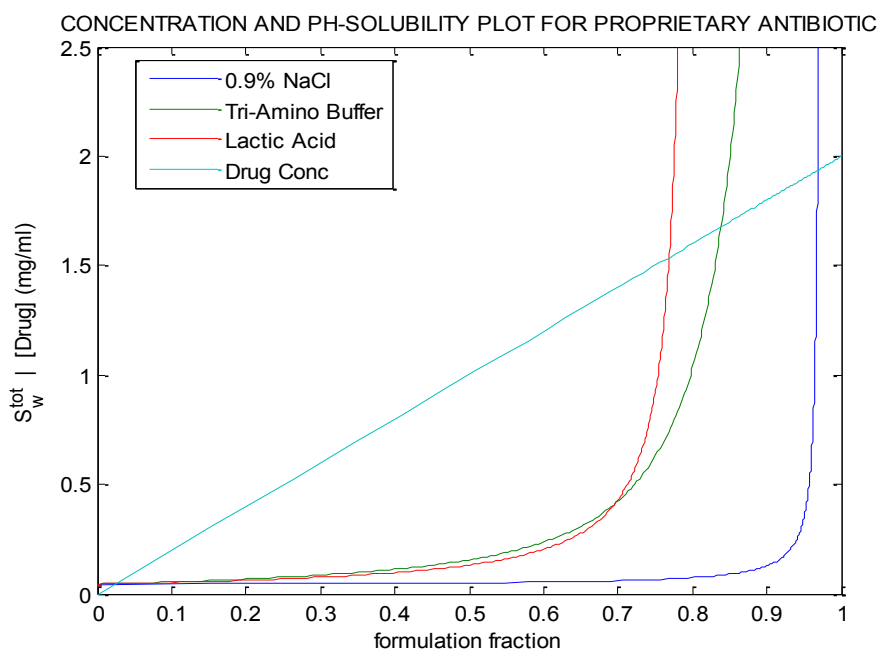


Figure 45. Drug concentration & solubility plot for the proprietary antibiotic

3.1.4.2. In Vitro Results

The results of the in vitro study are summarized in table 9 and figures 46 and 47. These results show that for the first minute of infusion the formulation containing 1.5mM of Tartaric Acid precipitates upon mixing with blood surrogate while the formulations with higher buffer concentrations do not.

Table 9. Calculated AUC values from the intensity plots

FORMULATION	NEEDLE TIP			DOWNSTREAM		
	AUC1	AUC2	AVG	AUC1	AUC2	AVG
Form1	422.50	357.50	390.00	3024.80	2885.60	2955.20
Form2	0.00	0.00	0.00	79.52	32.80	56.16
Form3	2.92	0.00	1.46	14.17	87.57	50.87

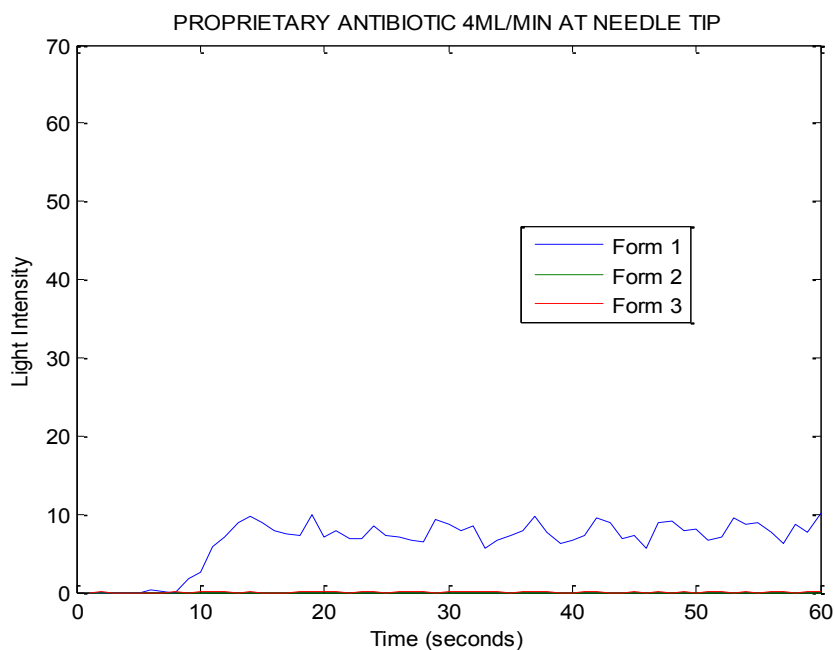


Figure 46 In vitro results for the proprietary antibiotic formulations

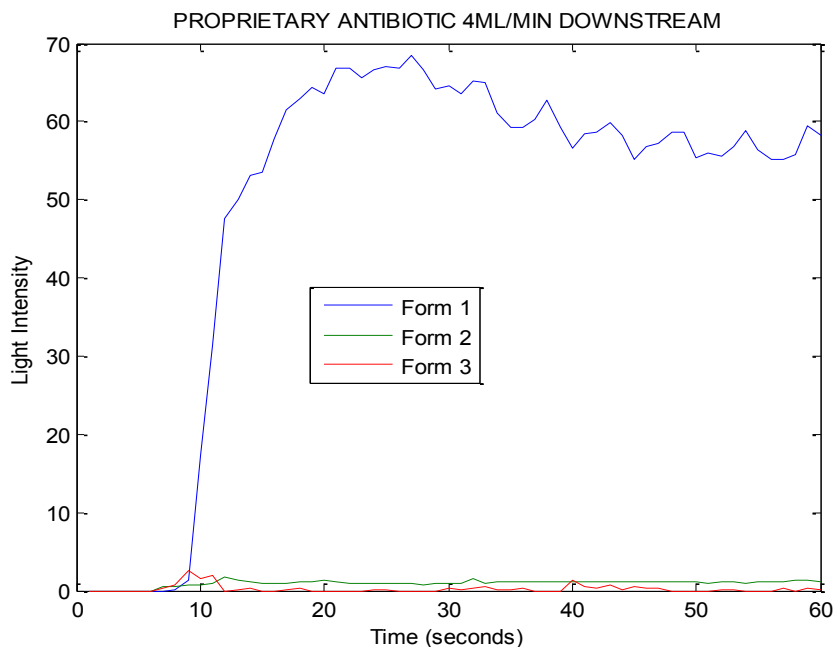


Figure 47. In vitro results for the proprietary antibiotic formulations

The scaled intensity images, shown in figures 48-51, are a visual comparison of the first and second formulations with respect to the amount of drug precipitated. Formulation 1 (figures 48 and 50) show a small amount of precipitation at the needle tip that increases as the formulation moves down the tube. The second formulation (figures 49 and 51) with higher buffer capacity shows no precipitation at the needle tip and downstream. By reducing the area of supersaturation for the proprietary antibiotic, the amount of drug precipitation for a one minute injection has been eliminated. The images of formulation 3 are identical to the images of formulation 2.

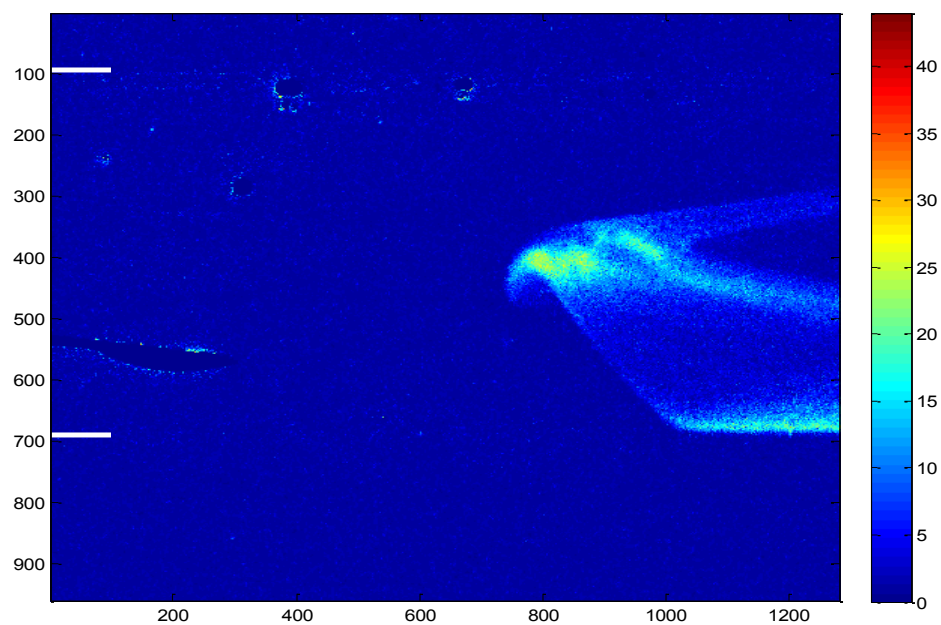


Figure 48. Image of proprietary antibiotic (form 1) at the needle tip

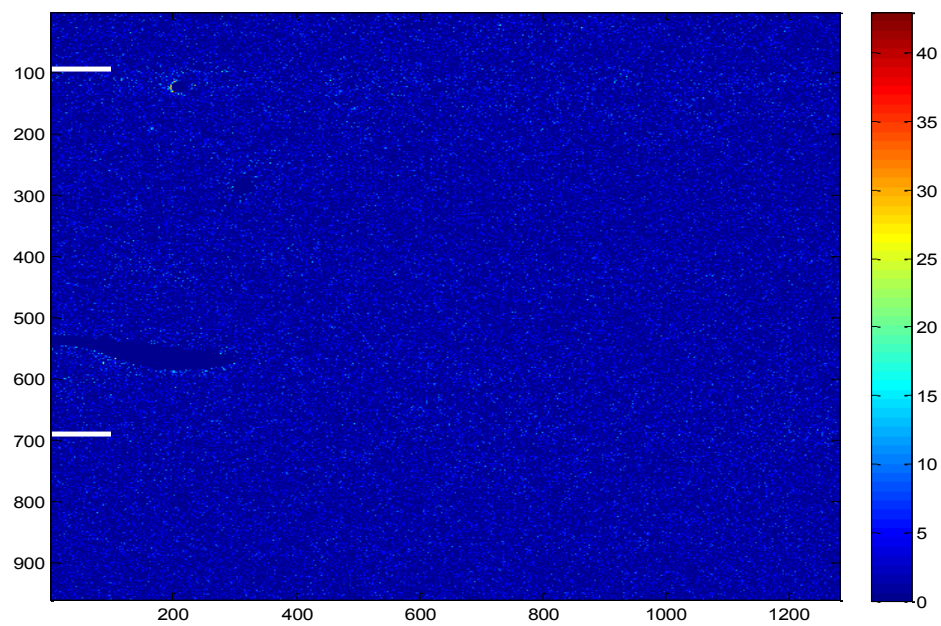


Figure 49. Image of the proprietary antibiotic (form 2) at the needle tip

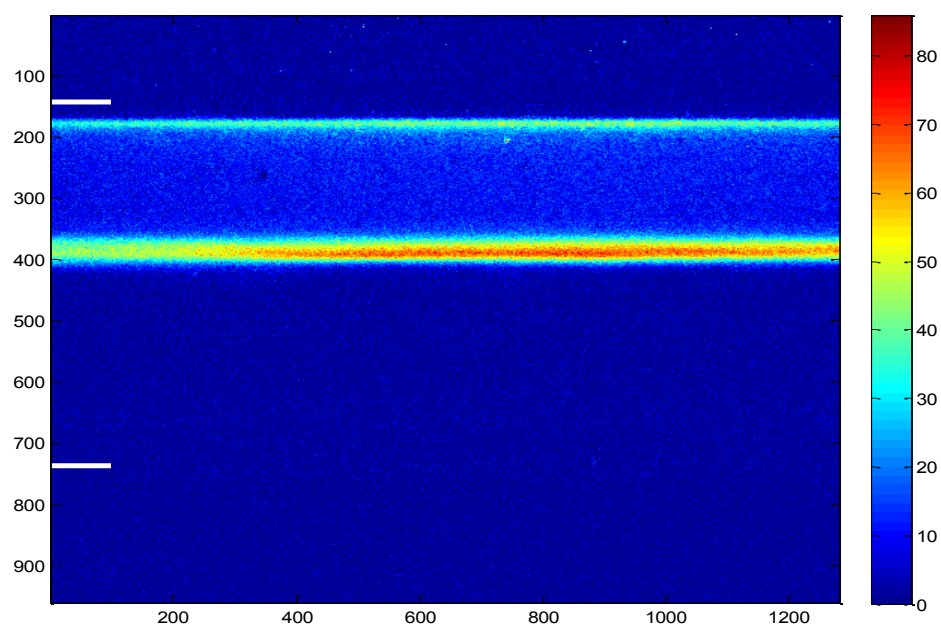


Figure 50. Image of the proprietary antibiotic (form 1) downstream

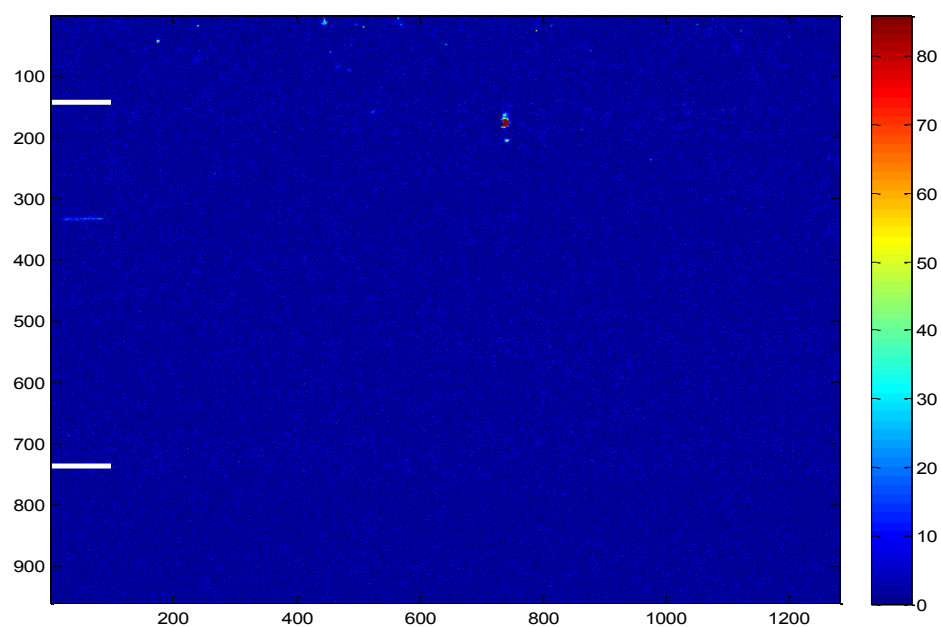


Figure 51. Image of the proprietary antibiotic (form 2) downstream

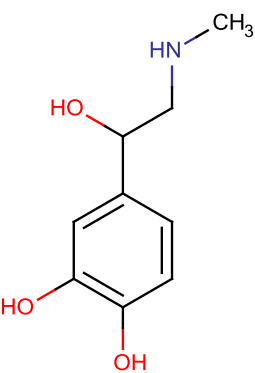
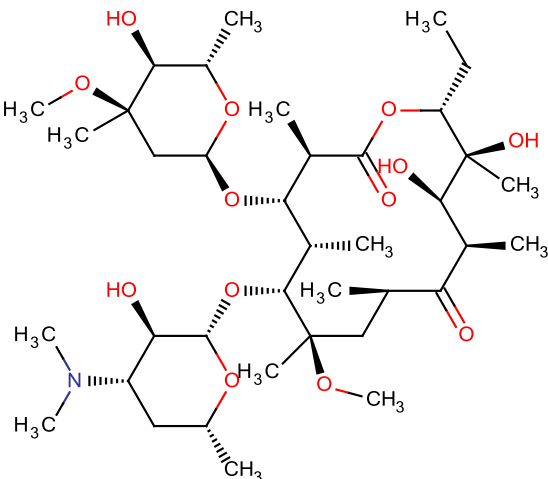
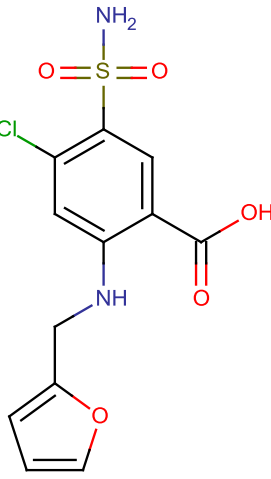
3.1.5. Non-Precipitating Drugs

All drug formulations listed in table 10 were formulated at concentrations that did not exceed the solubility of the drug at pH 7.4. The chemical structures for these three compounds are shown in table 11. Using the data in table 10 and the results of the previously used in vitro device (25), these formulations were not expected to show any precipitation upon dilution with blood surrogate.

Table 10. Negative control drugs used for testing the in vitro device

Drug	S_w	S_w^{tot} (pH=7.4)	pKa	[Formulation] (mg/ml)
Epinephrine	0.333 mg/ml (54)	5.49 mg/ml*	8.55 (55)	0.1 mg/ml (4)
Clarithromycin	2.95 μ g/ml* (56)	1.89 mg/ml*	9.20 (57)	1.3522 mg/ml (4)
Furosemide	0.018 mg/ml (58)	19.11 mg/ml*	3.80 (58)	10 mg/ml (4)
*Estimated from Henderson-Hasselbalch				

Table 11. Structures of epinephrine, clarithromycin, and furosemide

		
Epinephrine	Clarithromycin	Furosemide

3.1.5.1. In Vitro Results

Clarithromycin is another macrolide antibiotic used to treat a number of bacterial infections. The IV formulation contains the lactobionate salt of clarithromycin along with 0.9% sodium chloride and enough sodium hydroxide to bring the pH up to an unlisted value (4). The final concentration listed is 2mg/ml of the clarithromycin lactobionate salt. The pH chosen for this formulation was 5 because the stability of clarithromycin decreases exponentially for lower pH values (59). The results of the in vitro tests (figure 52) show that clarithromycin does not precipitate at either of the two injection rates or at the two flow cell imaging locations. The phlebitis associated with the clarithromycin formulation is therefore, most likely not from drug precipitation, but rather the interaction of the drug in solution with venous cell membranes (60).

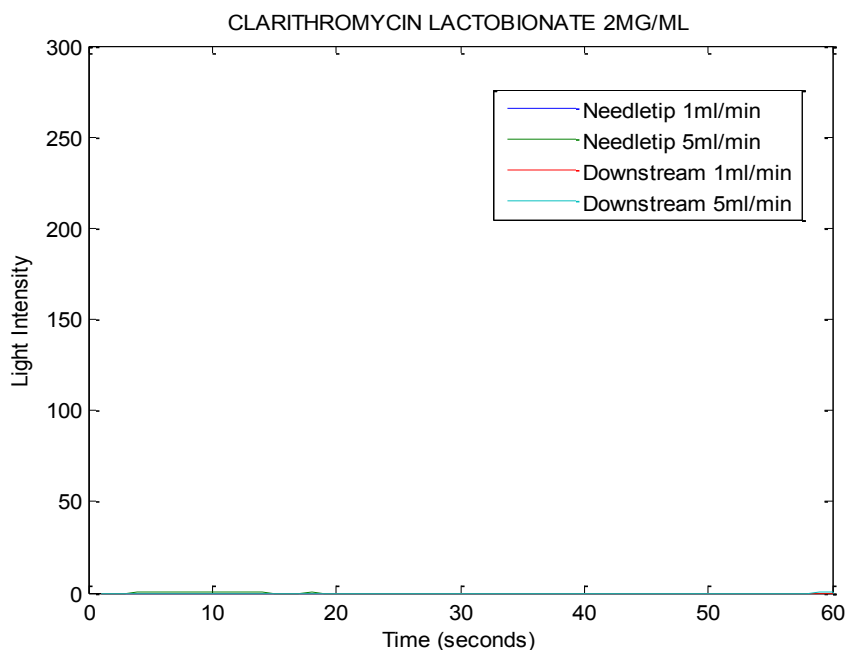


Figure 52. In vitro results for clarithromycin lactobionate

Epinephrine is a nonselective adrenergic agonist used in the treatment of anaphylaxis, asthma attacks, cardiac arrest, and transitory A-V heart block. The IV formulation contains sodium chloride as a tonicity agent, sodium metabisulfite as a preservative, and citric acid / sodium citrate as a buffer agent at pH 3.3 (4). When injected into the in vitro device, epinephrine did not precipitate regardless of injection rate or flow cell location. The spike in light intensity for the 5 ml/min injection between 20 and 30 seconds was a large air bubble that could not be subtracted from the results. The epinephrine used in IV formulations is the levo isomer, however, in this study racemic epinephrine was used. Because the melting point of the l-form (211-221⁰C) (61) and the dl-form (197-210⁰C) (62) (63) are not drastically different it is assumed that their intrinsic solubilities are similar.

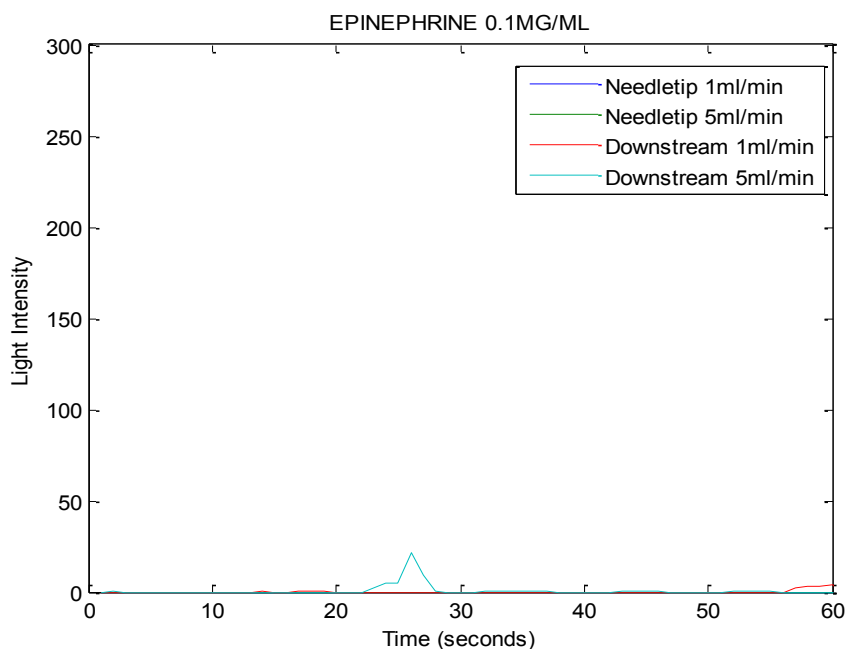


Figure 53. In vitro results for epinephrine

Furosemide is a loop diuretic primarily used in the treatment of conditions such as pulmonary edema and congestive heart failure. The furosemide IV formulation contains sodium chloride as a tonicity agent and sodium hydroxide or hydrochloric acid to bring the pH to 9 (4). The directions for use specify that a diluted IV dose that should not be given faster than 4mg/ml. To make the 1ml/min injection valid the concentration was reduced to 4mg/ml. Figure 54 is a plot of the in vitro results for the furosemide injections, showing no precipitation for both injections speeds and both flow cell locations.

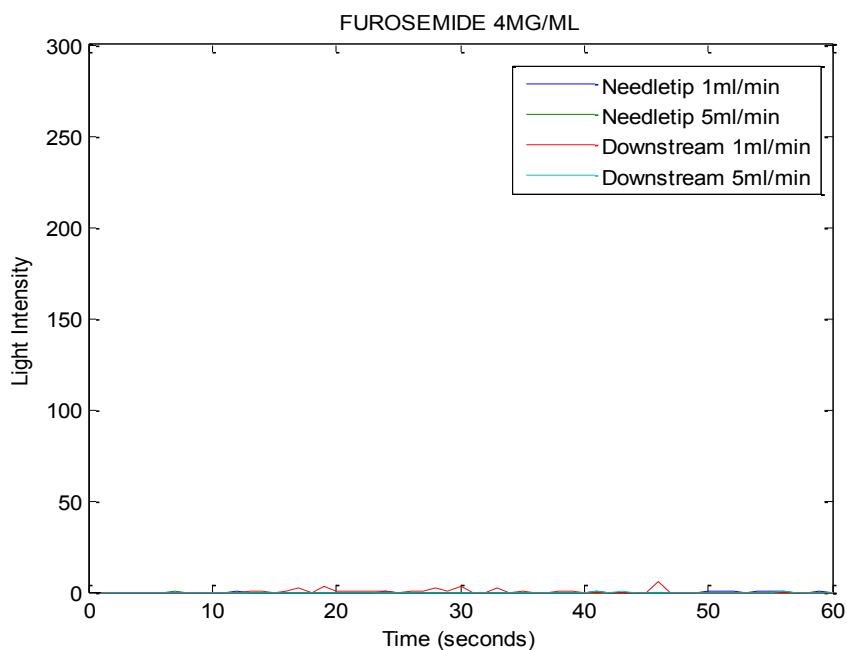


Figure 54. In vitro results for furosemide

3.2. Temperature Study

Increasing the temperature of the ISPB blood surrogate from 25⁰C to 37⁰C decreased the amount of precipitation for the amiodarone HCl formulation (figure 55), and the phenytoin sodium formulation (figure 56). The degree of precipitation for verapamil HCl at both 25⁰C and 37⁰C (figure 57) were approximately the same as the time approached one minute. The phenytoin formulation still produced solid drug crystals upon dilution, while precipitation from the amiodarone was thinner and more concentrated at the needle tip. Figures 58, 59, and 60 are the scaled intensity images of the 1ml/min injection of phenytoin, amiodarone, and verapamil, respectively. Because increasing the temperature reduced the amount of precipitation for two of the three drugs tested, it is suggested that for future studies, if a drug precipitates during in vitro testing at 25⁰C, the same drug should also be retested at 37⁰C.

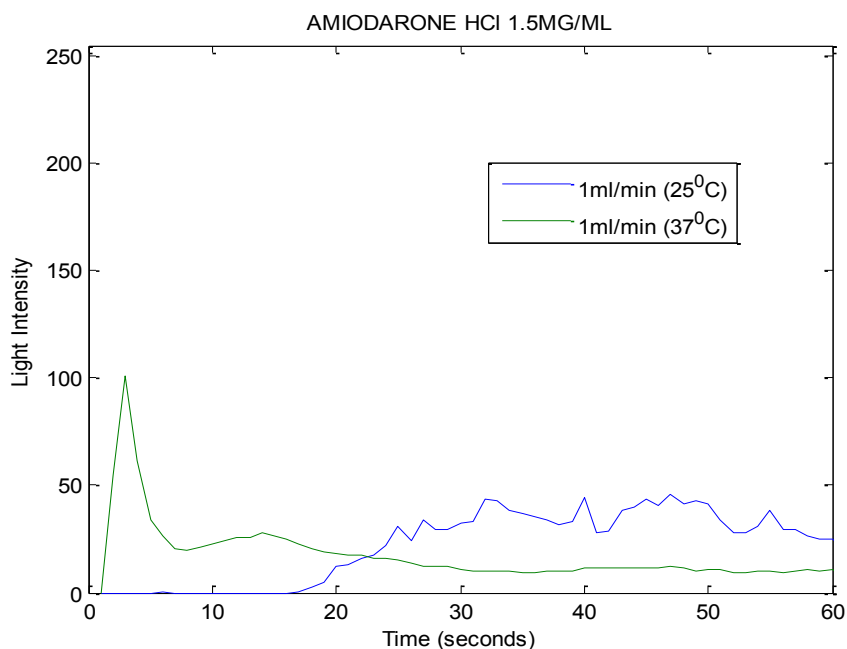


Figure 55. In vitro results for amiodarone HCl (ISPB at 25⁰C and 37⁰C)

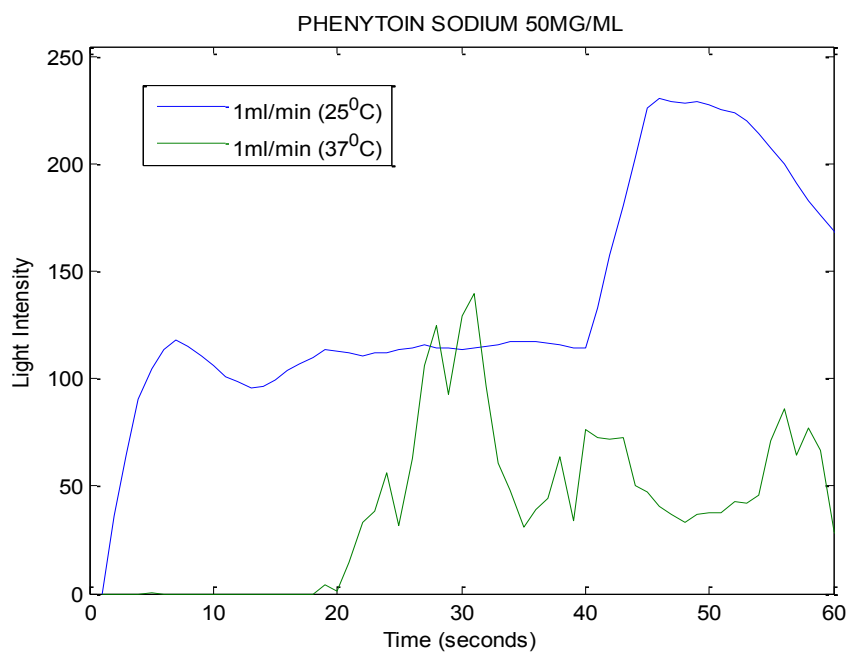


Figure 56. In vitro results for phenytoin sodium (ISPB at 25⁰C and 37⁰C)

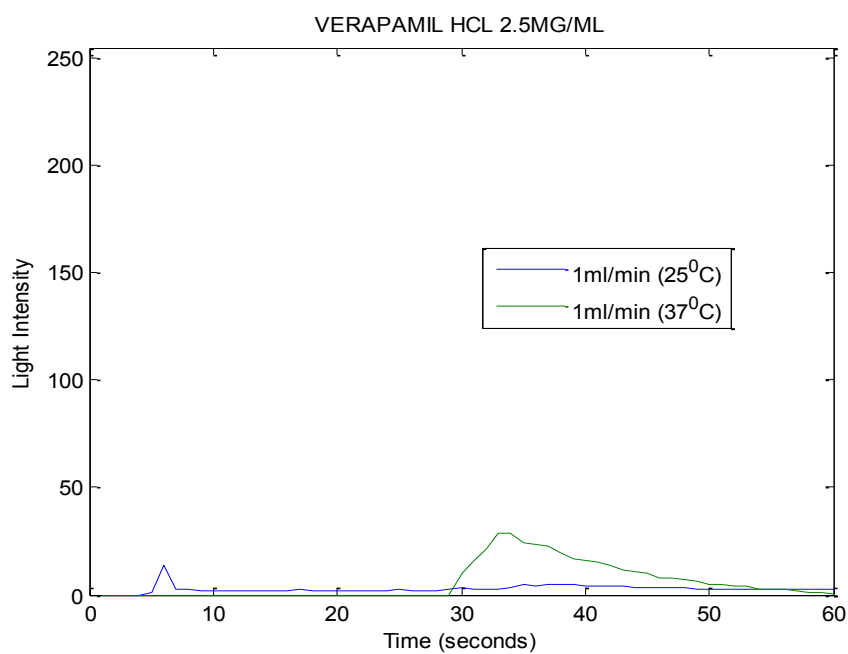


Figure 57. In vitro results for verapamil HCL (ISPB at 25⁰C and 37⁰C)

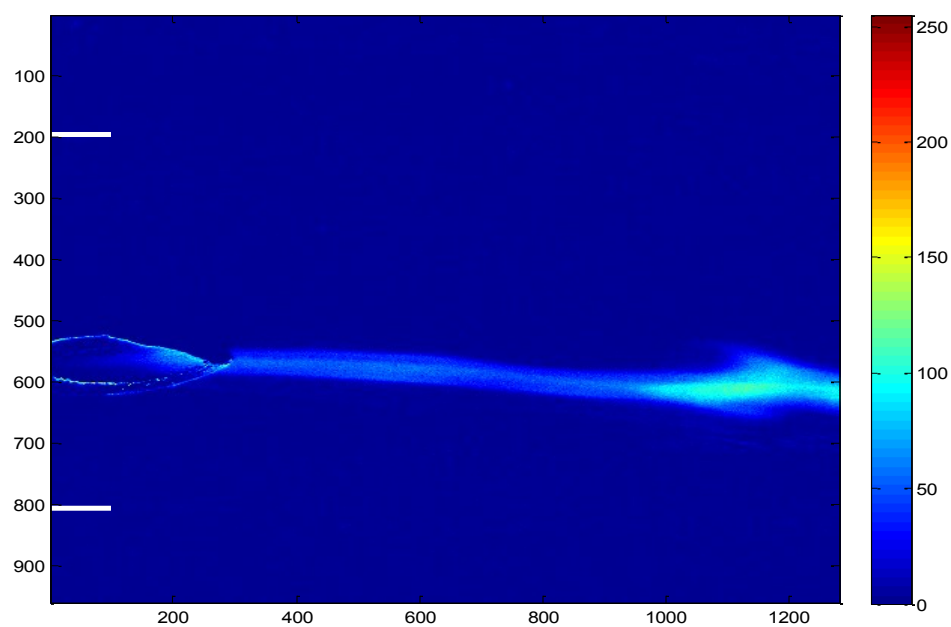


Figure 58. Image of the 1ml/min amiodarone HCl injection (ISPB at 37°C)

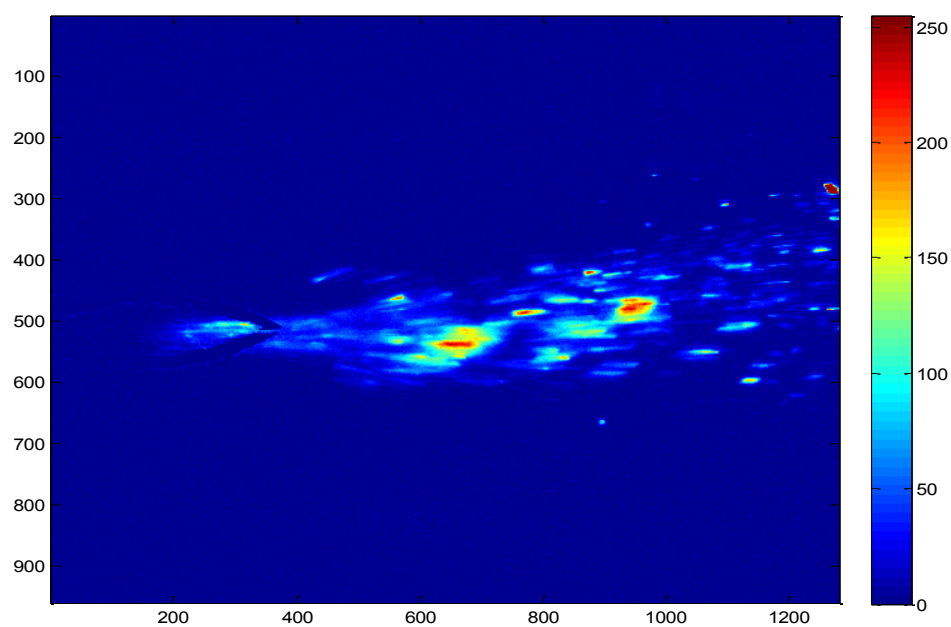


Figure 59. Image of 1ml/min phenytoin sodium injection (ISPB at 37°C)

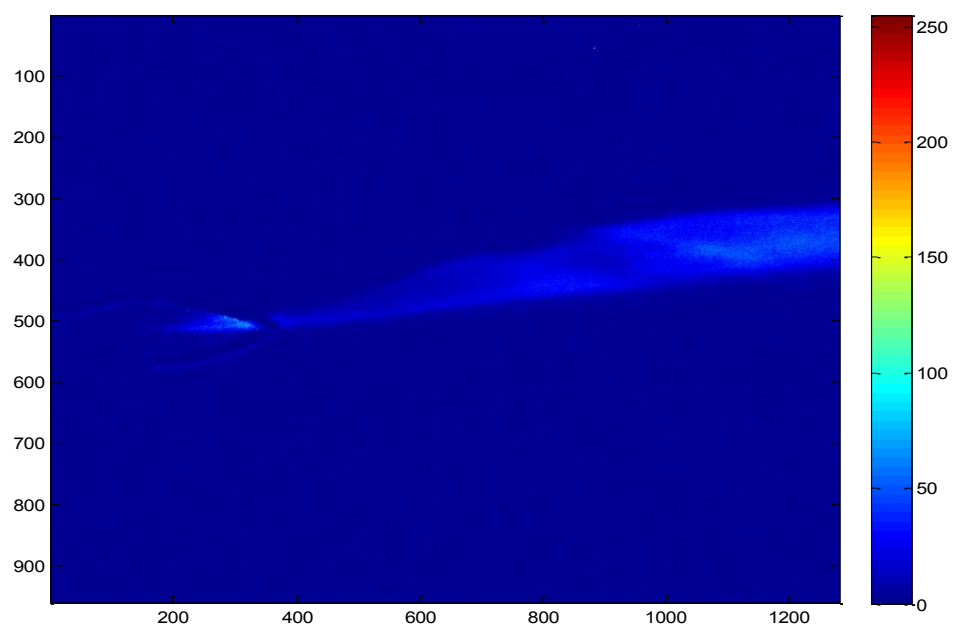


Figure 60. Image of the 1ml/min verapamil HCl injection (ISPB at 37⁰C)

SUMMARY

Detecting drug precipitation at the needle tip where phlebitis is observed is the main advantage of the in vitro device introduced in this work. Using the CCD camera and Matlab's[®] image processing toolbox made it possible to visualize the drug precipitation as it left the needle tip, or as the formulation mixed with blood downstream. The novel flow cell design allowed the use of a round quartz tube to model the forearm vein by reducing the amount of refracted light off the curved surface. For our blood model, performing the in vitro experiments with ISPB at 37⁰C reduced the amount of precipitation for two of the three drugs tested. Thus, future in vitro drug precipitation tests should include the use of ISPB at 37⁰C.

The software used in this work is able to build a formulation with commonly used excipients and can predict the total drug solubility using empirical and theoretical calculations. After this is done, the software predicts how the drug solubility will change as the formulation is mixed with blood upon administration. In this work the results obtained from the software, and the in vitro tests, were in good agreement with one another. As demonstrated for the proprietary antibiotic formulations, using the results of both the software, and the in vitro device, can greatly assist in finding the optimal formulation for a parenteral drug. In addition, these calculations and in vitro tests can be performed quickly and at relatively low cost compared to animal studies.

APPENDIX A – LIST OF CHEMICALS USED FOR THE IN VITRO STUDY

Table 12. Chemicals used for the in vitro study

Chemical	Manufacturer	Catalog #	Purity
5-5-Diphenylhydantoin	Sigma Chemical Co	D4007	99%
Citric Acid (Anhydrous)	Sigma Chemical Co	C1857	USP
Trisodium Citrate	Sigma Chemical Co	S4641	99.9%
Epinephrine (±)	Sigma Chemical Co	E1635	98%
Furosemide	Sigma Chemical Co	F4381	98%
Sodium Phosphate Dibasic	EMD Chemical Inc	SX0720-1	99.0%
Lactic Acid	Sigma Chemical Co	L6661	USP
Sodium Metabisulfite	Spectrum Chemical Co	S0182	USP/NF
Amiodarone HCl	Sigma Chemical Co	A8423	98%
Ethanol	Sigma-Aldrich Co	493546	USP
Propylene Glycol	J.T. Baker	U510-07	99.5%
Sodium Chloride	BDH (VWR International)	BDH0286	99.0%
Potassium Phosphate	Spectrum Chemical Co	P1380	99.0%
pH 2 Standard	EMD Chemical Inc	BX-1652-1	NIST
pH 4 Standard	EMD Chemical Inc	BX-1628-1	NIST
pH 7 Standard	EMD Chemical Inc	BX-1632-1	NIST
pH 2 Standard	EMD Chemical Inc	BX-1641-1	NIST
Benzyl Alcohol	Sigma Aldrich	108006	99%
Polysorbate 80	Spectrum Chemical Co	P1179	NL
Sodium Hydroxide	EM Science	SX0590-13	97%
Hydrochloric Acid	Sigma-Aldrich Co	285148	ACS
L-Histidine	University of Iowa Pharmaceuticals	NL	USP/EP
L-Glutamic Acid	University of Iowa Pharmaceuticals	NL	USP/EP
L-Aspartic Acid	University of Iowa Pharmaceuticals	NL	USP/EP
L-Tartaric Acid	Sigma-Aldrich Chemical Co	33801	99.5-101.0%
Clarithromycin	Sigma Chemical Co	C9742	95%
Lactobionic Acid	Aldrich Chemical Company	15,351-6	97%
Verapamil	Sigma Chemical Co	V-4629	99%
Dextrose 5%	Baxter	1A0063	USP

REFERENCES

1. Rowland, M.; Tozer, T. *Clinical Pharmacokinetics Concepts and Applications*, 3rd ed.; Lippincott Williams & Smith: Philadelphia, 1995.
2. Turco, S. J.; King, R. E. *Sterile Dosage Forms: Their Preparation and Clinical Application*, 2nd ed.; Lea & Febiger: Philadelphia, 1979.
3. Crane, V. S. Significance of osmoticity in antibiotic small-volume parenterals. *The Annals of Pharmacotherapy* **1987**, *21* (10), 830-834.
4. Trissel, L. *Handbook of Injectable Drugs*, 8th ed.; American Society of Health-System Pharmacists: Bethesda, 1994.
5. Nguyen, M. K.; Ornekian, V.; Butch, A. W.; Kurtz, I. A new method for determining plasma water content: application in pseudohyponatremia. *Am J Physiol Renal Physiol* **2007**, *292* (5), F1652-F1656.
6. Yalkowsky, S. H. *Solubility and Solubilization in Aqueous Media*, 1st ed.; Oxford University Press: New York, 1999.
7. Stahl, P.; Wermuth, C. *Pharmaceutical Salts: Properties, Selection, and Use*, 1st ed.; John Wiley and Sons: Hoboken, 2002.
8. Rubino, J. T. Cosolvents and Cosolvency. In *Encyclopedia of Pharmaceutical Technology*, 3rd ed.; J, S., Ed.; Taylor & Francis: New York, 2013; pp 806-819.
9. Yalkowsky, S. H. Solubilization of drugs by cosolvents. In *Techniques of Solubilization of Drugs*; SH, Y., Ed.; Marcel Dekker: New York, 1981; pp 91-134.
10. Elworthy, P. H.; Florence, A. T.; MacFarlane, C. B. *Solubilization by Surface Active Agents and its application in Chemistry and the Biological Sciences*; Chapman and Hall Ltd: London, 1968.
11. Veiga, M. D.; Diaz, P. J.; Fakhrul, A. Interactions of Griseofulvin with Cyclodextrins in Solid Binary Systems. *Journal of Pharmaceutical Sciences* **1998**, *87* (7), 891-900.
12. Geigy, D. *Scientific Tables*, 7th ed.; J.R. Geigy S.A.: Ardsley, 1970.
13. Surakitbanharn, Y.; Simamora, P.; Ward, G. H.; Yalkowsky, S. H. Precipitation of pH solubilized phenytoin. *International Journal of Pharmaceutics* **1994**, *109*, 27-33.

14. de Levie, R. A General Simulator for Acid-Base Titrations. *Journal of Chemical Education* **1999**, 76 (7), 987-991.
15. Karpinski, P. H.; Wey, J. S. Precipitation Processes. In *Handbook of Industrial Crystallization*, 2nd ed.; Myerson, A. S., Ed.; Butterworth-Heinemann: Woburn, 2001; pp 142-145.
16. DiMasi, J. M.; Hansen, R. W.; Grabowski, H. G. The price of innovation: new estimates of drug development costs. *Journal of Health Economics* **2003**, 22 (2), 151-185.
17. DiMasi, J. A.; Grabowski, H. G. The cost of biopharmaceutical R&D: is biotech different? *Managerial and Decision Economics* **2007**, 28 (4-5), 469-479.
18. Cohen, J.; Hubert, B.; Leeson, L.; Rhodes, C.; Robinson, J.; Theodore, R.; Shefler, E. The Development of USP Dissolution and Drug Release Standards. *Pharmaceutical Research* **1990**, 7 (10), 983-987.
19. Dai, W.-G. In vitro methods to assess drug precipitation. *International Journal of Pharmaceutics* **2010**, 393 (1-2), 1-16.
20. Box, G. E.; Draper, N. R. *Empirical Model-Building and Response Surfaces*, 1st ed.; John Wiley & Sons, Inc.: New York, 1987.
21. Schroeder, H. G.; DeLuca, P. B. A Study on the In Vitro Precipitation of Poorly Soluble Drugs from Nonaqueous Vehicles in Human Plasma. *Bull. Parenter. Drug Assoc* **1973**, 28, 1-14.
22. Li, P.; Vishnuvajjala, R.; Tabibi, S. E.; Yalkowsky, S. H. Evaluation of in Vitro Precipitation Methods. *Journal of Pharmaceutical Sciences* **1998**, 87 (2), 196-199.
23. Yalkowsky, S. H.; Valvani, S. C. Precipitation of solubilized drugs due to injection or dilution. *Drug Intelligence and Clinical Pharmacy* **1977**, 11, 417-419.
24. Yalkowsky, S. H.; Valvani, S. C.; Johnson, B. J. In vitro method for detecting precipitation of parenteral formulations after injection. *Journal of Pharmaceutical Sciences* **1983**, 72, 1014-1017.
25. Johnson, J. L.; Yalkowsky, S. H. Prediction of precipitation-induced phlebitis: A statistical validation of an in-vitro model. *Journal of Pharmaceutical Sciences* **2003**, 92, 1574-1581.

26. Simamora, P.; Pinsuwan, S.; Surakitbanharn, Y.; Yalkowsky, S. H. Studies in Phlebitis VIII: Evaluations of pH Solubilized Intravenous Dexverapamil Formulations. *PDA Journal of Pharmaceutical Science and Technology* **1996**, 50 (2), 123-128.
27. Myrdal, P. B.; Simamora, P.; Surakitbanharn, Y.; Yalkowsky, S. H. Studies in phlebitis. VII: In vitro and in vivo evaluation of pH-solubilized levemopamil. *Journal of Pharmaceutical Sciences* **1995**, 84, 849–852.
28. Narazaki, R.; Sanghvi, R.; Yalkowsky, S. H. Estimation of Drug Precipitation upon Dilution of pH–Cosolvent Solubilized Formulations. *Chemical Pharmaceutical Bulletin* **2007**, 55, 1203-1206.
29. Narazaki, R.; Sanghvi, R.; Yalkowsky, S. H. Estimation of Drug Precipitation upon Dilution of pH-Controlled Formulations. *Molecular Pharmaceutics* **2007**, 4 (4), 550-555.
30. Baptista-Silva, J.; Dias, A.; Cricenti, S.; Burihan, E. Anatomy of the Basilic Vein in the Arm and its Importance for Surgery. *Brazilian Journal of Morphological Sciences* **2003**, 20 (3), 171-175.
31. Comelli, F.; Ottani, S. Densities, Viscosities, Refractive Indices, and Excess Molar Enthalpies of Binary Mixtures Containing Poly(ethylene glycol)200 and 400 + Dimethoxymethane and + 1,2-Dimethoxyethane at 298.15 K. *Journal of Chemical Engineering Data* **2002**, 47 (5), 1226-1231.
32. Malitson, I. H. Interspecimen Comparison of the Refractive Index of Fused Silica. *Journal of The Optical Society of America* **1965**, 55 (10), 1205-1208.
33. ChemAxon. ChemAxon chemicalize.org beta. <http://www.chemicalize.org> (accessed Dec 26, 2013).
34. Slim, A. M.; Roth, J. E.; Duffy, B.; Rubal, B. J. The incidence of phlebitis with intravenous amiodarone at guideline dose recommendations. *Military Medicine* **2007**, 172 (12), 1279-1283.
35. Genne, D.; Siegrist, H. H.; Humair, L.; Janin-Jaquat, B.; deTorrente, A. Clarithromycin versus Amoxicillin-Clavulanic Acid in the Treatment of Community-Acquired Pneumonia. *European Journal of Clinical Microbiology and Infectious Diseases* **1997**, 16 (11), 783-788.

36. Jamerson, B. D.; Dukes, G. E.; Brouwer, K.; Dorm, K. H.; Messenheimer, J. A.; Powell, J. R. Venous Irritation Related to Intravenous Administration of Phenytoin versus Fosphenytoin. *Pharmacotherapy: The Journal of Human Pharmacology and Drug Therapy* **1994**, *14* (1), 49-52.
37. Simamora, P.; Pinsuwan, S.; Surakitbanharn, Y.; Yalkowsky, S. H. Studies in Phlebitis VIII: Evaluations of pH Solubilized Intravenous Dexverapamil Formulations. *PDA Journal of Pharmaceutical Science and Technology* **1996**, *50* (2), 123-128.
38. Ellison, G.; Straumfjord, J. V.; Hummel, J. P. Buffering Capacities of Human Blood and Plasma. *Clinical Chemistry* **1958**, *4*, 452-461.
39. Davio, S. R.; McShane, M. M.; Kakuk, T. J.; Zaya, R. M.; Cole, S. L. Precipitation of the Renin Inhibitor Ditekiren Upon iv Infusion; in Vitro Studies and Their Relationship to in Vivo Precipitation in the Cynomolgus Monkey. *Pharmaceutical Research* **1991**, *8* (1), 80-83.
40. Mehanna, A. S. Drugs Affecting the Cardiovascular System-Cardiac Agents: Cardiac Glycosides, Antianginal, and Antiarrhythmic Drugs. In *Foye's Principles of Medicinal Chemistry*, 6th ed.; Lemke, T. L., Williams, D. A., Roche, V. A., Zito, S. W., Eds.; Lippincott Williams & Wilkins: Baltimore, 2008; p 718.
41. Bonati, M.; Gaspari, F.; D'Aranno, V.; Benfenati, E.; Neyroz, P. Physiochemical and Analytical Characteristics of Amidoarone. *Journal of Pharmaceutical Sciences* **1984**, *73* (6), 829-831.
42. Bergstrom, C. A.; Luthman, K.; Artursson, P. Accuracy of calculated pH-dependent aqueous drug solubility. *European Journal of Pharmaceutical Sciences* **2004**, *22*, 387-398.
43. Alvarez-Núñez, F. A.; Yalkowsky, S. H. Relationship between Polysorbate 80 solubilization descriptors and octanol–water partition coefficients of drugs. *International Journal of Pharmaceutics* **2000**, *200* (2), 217-222.
44. Boyce, B. A.; Yee, B. H. Incidence and severity of phlebitis in patients receiving peripherally infused amiodarone. *Critical Care Nurse* **2012**, *32* (4), 27-34.
45. LeDuc, B. Drug Affecting the Central Nervous System-Antiseizure Drugs. In *Foyes Principles of Medicinal Chemistry*, 6th ed.; Lemke, T., Williams, D. A., Roche, V. F., Zito, S. W., Eds.; Lippincott Williams & Wilkins: Baltimore, 2008; pp 529-530.

46. Earnest, M.; Marx, J. A.; Lawrence, R. D. Complications of Intravenous Phenytoin for Acute Treatment of Seizures: Recommendations for Usage. *Journal of the American Medical Association* **1983**, 249 (6), 762-765.
47. Nokhodch, A.; Bolourtchian, N.; Dinarvand, R. Crystal modification of phenytoin using different solvents and. *International Journal of Pharmaceutics* **2003**, 250, 85-97.
48. Schwartz, P. A.; Rhodes, C. T.; Cooper Jr., J. W. Solubility and Ionization Characteristics of Phenytoin. *Journal of Pharmaceutical Sciences* **1977**, 66 (7), 994-997.
49. Millard, J.; Alvarez-Núñez, F. A.; Yalkowsky, S. H. Solubilization by cosolvents: Establishing useful constants for the log-linear model. *International Journal of Pharmaceutics* **2002**, 245 (1-2), 153-166.
50. Serajuddin, A.; Jarawski, C. Influence of pH on Release of Phenytoin Sodium from Slow-Release Dosage Forms. *Journal of Pharmaceutical Sciences* **1993**, 82 (3), 306-310.
51. Singh, B. N.; Ellrodt, G.; Peter, C. T. Verapamil: A Review of its Pharmacological Properties and Therapeutic Use. *Drugs* **1978**, 15 (3), 169-197.
52. Yoshida, M. I.; Gomes, E. C. L.; Soares, C. D. V.; Cunha, A. F.; Oliveira, M. A. Thermal Analysis Applied to Verapamil Hydrochloride Characterization in Pharmaceutical Formulations. *Molecules* **2010**, 15, 2439-2452.
53. Box, K. J.; Volgy, G.; Baka, E.; Stuart, M.; Takacs-Novak, K.; Comer, J. Equilibrium versus Kinetic Measurements of Aqueous Solubility, and the Ability of Compounds to Supersaturate in Solution—A Validation Study. *Journal of Pharmaceutical Sciences* **2006**, 95 (6), 1298-1307.
54. Chen, X.; Cho, S. J.; Li, Y.; Venkatesh, S. Prediction of aqueous solubility of organic compounds using a quantitative structure-property relationship. *Journal of Pharmaceutical Sciences* **2002**, 91 (8), 1838-1852.
55. Higuchi, T.; Schroeter, L. C. Kinetics and Mechanism of Formation of Sulfonate from Epinephrine and Bisulfite. *Journal of the American Chemical Society* **1960**, 82 (8), 1904-1907.

56. Pelta, M. D.; Boote, V.; Morris, G. A.; Barber, J. Acid-Catalyzed Degradation of Clarithromycin and Erythromycin B: A Comparative Study Using NMR Spectroscopy. *Journal of Medicinal Chemistry* **2000**, *43* (3), 467-474.
57. Goddard, A.; Jessa, M.; Barrett, D.; Shaw, P.; Idstrom, J.; Cederberg, C.; Spiller, R. Effect of omeprazole on the distribution of metronidazole, amoxicillin, and clarithromycin in human gastric juice. *Gastroenterology* **1996**, *111* (2), 358-367.
58. Manderscheid, M.; Eichinger, T. Determination of pKa Values by Liquid Chromatography. *Journal of Chromatographic Science* **2003**, *41*, 323-326.
59. Nakagawa, Y.; Itai, S.; Yoshida, T.; Nagai, T. Physiochemical Properties and Stability in the Acidic Solution of a New Macrolide Antibiotic, Clarithromycin, in Comparison with Erythromycin. *Chemical and Pharmaceutical Bulletin* **1992**, *40* (3), 725-728.
60. Vorbach, H.; Weigel, G.; RobibaroO, B.; Armbruster, C.; Schaumann, R.; Hlousek, M.; Reiter, M.; Griesmacher, A.; Georgopoulos, A. Endothelial cell compatibility of clarithromycin for intravenous use. *Clinical Biochemistry* **1998**, *31* (8), 653-656.
61. Windholz, M., Budavari, S., Stroumtsos, L. Y., Fertig, M. N., Eds. *The Merck Index*, Ninth ed.; Merck & Co. Inc.: Rahway, 1976.
62. Sigma Aldrich Co. Sigma Aldrich Website.
<http://www.sigmaaldrich.com/catalog/product/sigma/e1635?lang=en®ion=US>
(accessed Jan 4, 2014).
63. MP Biomedicals, LLC. MP Biomedicals Web site.
<http://www.mpbio.com/product.php?pid=02151064&country=223> (accessed Jan 4, 2014).